Center-of-mass momentum dependence of short-range correlations with the coarse-grained Granada potential

P. R. Casale,[1] J. E. Amaro,[2,*] E. Ruiz Arriola,[2] and I. Ruiz Simo[2,†]

[1]*Departamento de Física Atómica, Molecular y Nuclear, Universidad de Granada, E-18071 Granada, Spain*

[2]*Departamento de Física Atómica, Molecular y Nuclear and Instituto Interuniversitario Carlos I de Física Teórica y Computacional, Universidad de Granada, E-18071 Granada, Spain*

(Received 21 June 2023; accepted 19 October 2023; published 6 November 2023)

The effect of the center-of-mass motion on the high-momentum distributions of correlated nucleon pairs is studied by solving the Bethe-Goldstone equation in nuclear matter with the Granada nucleon-nucleon potential. We show that this coarse-grained potential reduces the problem to an algebraic linear system of five (ten) equations for uncoupled (coupled) partial waves that can be easily solved. The corresponding relative wave functions of correlated *pn*, *pp*, and *nn* pairs are computed for different values of their center-of-mass (CM) momentum. We find that the *pn* pairs dominate the high-momentum tail of the relative momentum distribution, and that this only depends marginally on center-of-mass momentum. Our results provide further justification and agreement for the factorization approximation commonly used in the literature. This approximation assumes that the momentum distribution of nucleon pairs can be factorized as the product of the center-of-mass momentum distribution and the relative momentum distribution.

DOI: 10.1103/PhysRevC.108.054001

I. INTRODUCTION

The nucleon-nucleon (N-N) correlations and the attempts to reduce it to a problem of self-consistent fields, similar to the Hartree method [1,2] of atomic physics, constitute an old topic in nuclear physics [3–10]. It has experienced a revival in the last two decades due to the advent of high energy electron beams accelerators facilities such as the Continuous Electron Beam Accelerator Facility (CEBAF) at Jefferson Lab (JLab) [11,12], from both the experimental [13–29] and theoretical [30–68] points of view (for recent reviews the reader is referred to [69–72]).

From the theoretical side, the short-range N-N correlations (SRCs) are very important in different contexts of nuclear physics, covering aspects from fundamental to applied nuclear physics: properties of nuclear matter [31,39,73–75]; high momentum components in the nuclear wave function [35,47,50,76–78]; implications in nuclear astrophysics and evolution of neutron stars through the equation of state of nuclear and neutron matter [44,79–83]; calculations of symmetry energy and pairing gaps in nuclear and neutron matter [53,62,66,84]; models of relativistic heavy-ion collisions [85]; calculations of nuclear matrix elements for neutrinoless double beta decay [86,87]; description of (e, e'), $(e, e'N)$, and $(e, e'NN)$ reactions [33,37,38,45,56]; and, recently, the universality of the N-N SRCs and its connection with factorization properties of the nuclear wave functions and momentum distributions, and with the nuclear contacts [57,58,88–94], just to mention a few of them.

Traditionally, there have been two main methods to tackle this complex problem: the use of Jastrow correlation functions with adequate behaviors at short and long internucleon distances applied to Slater determinants of single-particle wavefunctions within variational approaches [5,34,37,49,95–102]; and the Brueckner theory of nuclear matter [9,103,104] by solving the Bethe-Goldstone (B-G) equation [7,105,106] or the effective interaction encoded in the G-matrix formalism [107–113].

There are also other useful methods to deal with this problem: the similarity renormalization group (SRG) methods, which can provide phase equivalent potentials that soften the short-range interaction, thus avoiding the problems related with the hard core [55,114,115]; and the *ab initio* variational Monte Carlo methods, which solve exactly the nonrelativistic many-body problem for light nuclei when a particular N-N interaction is given [116–121].

Our aim in this work is to extend our two previous papers [63,68] on the short-range correlations in the independent pair approximation picture [122] for the case when the total center-of-mass (CM) momentum of the nucleon pair is different from zero, $\mathbf{K}_{\rm CM} \neq \mathbf{0}$, and to study its effect on the high-momentum components of the relative wave function in momentum space. To this end we make use of the coarse-grained Granada potential of Ref. [123], and we use the angular average of the Pauli-blocking operator appearing in the B-G equation. This approximation has been widely used in the past by many other authors [9,36,108,109,124–126]. Other successful attempts to solve this problem without resorting to the approximation of

*amaro@ugr.es

†Corresponding author: ruizsig@ugr.es

the angular average of the Pauli-blocking operator have been explored in Refs. [127–133].

Given the fact that the coordinate space method is not widely used and it is essential for our coarse-grained treatment of the N-N interaction, we provide in two appendices all the necessary material to make the paper as self-contained as possible, in order to target it at a wider audience.

Therefore, the structure of this paper is as follows: in Sec. II we describe the formalism to solve the B-G equation with the angular average of the Pauli-blocking operator by performing a partial wave expansion for the radial part of the correlated relative wave function. In Sec. III we derive the correlated wave function in momentum space by applying the Fourier transform to the wave function in coordinate representation, and obtaining the high-momentum components in the relative wave function induced by the SRCs. In Sec. IV we present our results and discuss them in depth. In Sec. V we draw our conclusions. Finally, we provide Appendices A and B at the end of the paper.

II. THEORETICAL FRAMEWORK

A. General formalism

The Brueckner reaction matrix G plays a crucial role in describing nucleon-nucleon scattering within the nuclear medium. It is a fundamental concept in nuclear many-body theory, and its properties are closely related to the Bethe-Goldstone equation. The G matrix is a solution to the Bethe-Goldstone equation and is essentially a modified nucleon-nucleon scattering matrix that takes into account the influence of the nuclear medium on nucleon interactions. It can be thought of as a generalization of the Lippmann-Schwinger equation, which is commonly used to describe scattering in vacuum.

The Brueckner G matrix is usually represented in operator form as the well-known B-G equation:

$$G = V + V\,\frac{Q}{E - H_0}\,G, \tag{1}$$

where G is the G matrix or effective interaction; V represents the nucleon two-body potential; Q is the Pauli-blocking operator that prevents scattering over two-particle occupied states; E represents the energy eigenvalue of the two-nucleon system; and, finally, H_0 is the unperturbed or free Hamiltonian containing the sum of the kinetic energies of the two independent particles. The action of the Pauli-blocking operator over uncorrelated two-particle states $|\mathbf{k}_1, \mathbf{k}_2\rangle$ is given by

$$Q|\mathbf{k}_1, \mathbf{k}_2\rangle = \begin{cases} |\mathbf{k}_1, \mathbf{k}_2\rangle & \text{if both } |\mathbf{k}_i| > k_F \\ 0 & \text{otherwise.} \end{cases} \tag{2}$$

It is well known that due to translational invariance symmetry [134], if the N-N potential only depends on the relative coordinate $\mathbf{r}$ of the two-nucleon system and not on the CM coordinate $\mathbf{R}_{\rm CM}$, then the CM momentum of the two-nucleon system is conserved, i.e., it is a constant of motion. This means in practice that the CM motion can be described by a plane wave in nuclear matter, and that the correlated total wave function is separable into a product of a plane wave for the CM motion and a correlated relative wave function, $\psi_{\mathbf{K}_{\rm CM},\mathbf{k}}(\mathbf{r})$, depending explicitly on the relative coordinate $\mathbf{r}$, the initial relative momentum $\mathbf{k}$, and also on the total momentum $\mathbf{K}_{\rm CM}$ of the nucleon pair (see, for instance, Refs. [63,134]). The dependence on the total momentum $\mathbf{K}_{\rm CM}$ of the nucleon pair in the relative wave function can be understood if one observes that the Pauli-blocking operator Q explicitly depends on the CM momentum in the eigenket representation of CM and relative momenta for the two-nucleon system $|\mathbf{K}_{\rm CM}, \mathbf{k}\rangle$. The relationships between these two different representations for the two-nucleon system are given by

$$\begin{aligned}
\mathbf{R}_{\rm CM} &= \frac{1}{2}(\mathbf{r}_1 + \mathbf{r}_2), \quad \mathbf{K}_{\rm CM} = \mathbf{k}_1 + \mathbf{k}_2, \\
\mathbf{r} &= \mathbf{r}_1 - \mathbf{r}_2, \quad \mathbf{k} = \frac{1}{2}(\mathbf{k}_1 - \mathbf{k}_2), \\
\langle \mathbf{R}_{\rm CM}, \mathbf{r}\,|\mathbf{r}_1, \mathbf{r}_2\rangle &= \delta^3\left(\mathbf{R}_{\rm CM} - \frac{1}{2}(\mathbf{r}_1 + \mathbf{r}_2)\right) \\
&\quad \times \delta^3(\mathbf{r} - (\mathbf{r}_1 - \mathbf{r}_2)), \\
\langle \mathbf{K}_{\rm CM}, \mathbf{k}\,|\mathbf{k}_1, \mathbf{k}_2\rangle &= \delta^3\left(\mathbf{k}_1 - \mathbf{k} - \frac{\mathbf{K}_{\rm CM}}{2}\right) \\
&\quad \times \delta^3\left(\mathbf{k}_2 + \mathbf{k} - \frac{\mathbf{K}_{\rm CM}}{2}\right) \\
&= \delta^3(\mathbf{K}_{\rm CM} - (\mathbf{k}_1 + \mathbf{k}_2)) \\
&\quad \times \delta^3\left(\mathbf{k} - \frac{1}{2}(\mathbf{k}_1 - \mathbf{k}_2)\right), \\
\langle \mathbf{R}_{\rm CM}, \mathbf{r}\,|\mathbf{K}_{\rm CM}, \mathbf{k}\rangle &= \langle \mathbf{r}_1, \mathbf{r}_2\,|\mathbf{k}_1, \mathbf{k}_2\rangle = \frac{e^{i\,\mathbf{k}_1\cdot\mathbf{r}_1}}{(2\pi)^{\frac{3}{2}}}\,\frac{e^{i\,\mathbf{k}_2\cdot\mathbf{r}_2}}{(2\pi)^{\frac{3}{2}}} \\
&= \frac{e^{i\,\mathbf{K}_{\rm CM}\cdot\mathbf{R}_{\rm CM}}}{(2\pi)^{\frac{3}{2}}}\,\frac{e^{i\,\mathbf{k}\cdot\mathbf{r}}}{(2\pi)^{\frac{3}{2}}}.
\end{aligned} \tag{3}$$

The advantage of using the CM and relative momenta representation for initial and final two-nucleon states $|\mathbf{K}_{\rm CM}, \mathbf{k}\rangle$ is based on the fact that then the Brueckner G matrix can be solved solely for the relative wave function, at the price of introducing a dependence on the total momentum $\mathbf{K}_{\rm CM}$ through the Pauli-blocking operator Q. But the SRCs are completely incorporated in the relative wave function $\psi_{\mathbf{K}_{\rm CM},\mathbf{k}}(\mathbf{r})$.

On the other hand, if one insists on working with the two-nucleon momenta eigenket representation $|\mathbf{k}_1, \mathbf{k}_2\rangle$, the action of the Pauli-blocking operator on these states is much simpler [see Eq. (2)], but then one spoils the simplicity of the N-N potential matrix elements in the CM and relative coordinates representation,

$$\langle \mathbf{R}'_{\rm CM}, \mathbf{r}'|V|\mathbf{R}_{\rm CM}, \mathbf{r}\rangle = \delta^3(\mathbf{R}'_{\rm CM} - \mathbf{R}_{\rm CM})\,V(\mathbf{r})\,\delta^3(\mathbf{r}' - \mathbf{r}), \tag{4}$$

if the potential is, additionally, local in the relative coordinate, as the one we use in this work and in our previous ones [63,68,123,135]. Furthermore, with the latter approach one has to self-consistently solve the B-G equation for a correlated two-body wave function, $\Psi(\mathbf{r}_1, \mathbf{r}_2)$, depending on the coordinates and quantum numbers of the single nucleons (see for example Eq. (3) of Ref. [63]), instead of solving a one-body relative wave function with external inputs $(\mathbf{K}_{\rm CM}, \mathbf{k})$ in a single relative coordinate $\psi_{\mathbf{K}_{\rm CM},\mathbf{k}}(\mathbf{r})$.

The B-G equation in operator form, given in Eq. (1), is equivalent to the following equation for the perturbed or correlated two-nucleon state:

$$|\Psi_{\mathbf{K}_{\rm CM},\mathbf{k}}\rangle = |\mathbf{K}_{\rm CM},\mathbf{k}\rangle + \int d^3K'_{\rm CM}\, d^3k'\, \frac{Q(\mathbf{K}'_{\rm CM},\mathbf{k}')}{\frac{(\mathbf{K}^2_{\rm CM}-\mathbf{K}'^2_{\rm CM})}{2M_T}+\frac{(\mathbf{k}^2-\mathbf{k}'^2)}{2\mu}} \times \left|\frac{\mathbf{K}'_{\rm CM}}{2}+\mathbf{k}',\frac{\mathbf{K}'_{\rm CM}}{2}-\mathbf{k}'\right\rangle\langle\mathbf{K}'_{\rm CM},\mathbf{k}'|V|\Psi_{\mathbf{K}_{\rm CM},\mathbf{k}}\rangle, \tag{5}$$

where $|\mathbf{K}_{\rm CM},\mathbf{k}\rangle$ is the unperturbed or uncorrelated state, and $Q(\mathbf{K}'_{\rm CM},\mathbf{k}')$ is the Pauli-blocking operator depending on the CM and relative momenta and is given by

$$Q(\mathbf{K}'_{\rm CM},\mathbf{k}') = \theta\left(\left|\frac{\mathbf{K}'_{\rm CM}}{2}+\mathbf{k}'\right|-k_F\right)\theta\left(\left|\frac{\mathbf{K}'_{\rm CM}}{2}-\mathbf{k}'\right|-k_F\right), \tag{6}$$

with $\theta(x)$ the Heaviside or step function. Additionally, in Eq. (5), $\mu=\frac{M_N}{2}$ is the reduced mass of the two-nucleon system and $M_T=2M_N$ is its total mass. Finally, the integration over the off-shell states runs over the total CM and relative momenta of the two-nucleon pair. It is also important to notice that, despite its dependence, the ket $|\frac{\mathbf{K}'_{\rm CM}}{2}+\mathbf{k}',\frac{\mathbf{K}'_{\rm CM}}{2}-\mathbf{k}'\rangle$ is not a ket belonging to the CM and relative momenta representations, as they are, for instance, $|\mathbf{K}_{\rm CM},\mathbf{k}\rangle$ or $\langle\mathbf{K}'_{\rm CM},\mathbf{k}'|$, but it is a ket belonging to the two-nucleon single momenta representation $|\mathbf{k}_1,\mathbf{k}_2\rangle$ with $\mathbf{k}_1=\frac{\mathbf{K}'_{\rm CM}}{2}+\mathbf{k}'$ and $\mathbf{k}_2=\frac{\mathbf{K}'_{\rm CM}}{2}-\mathbf{k}'$.

The formal derivation of Eqs. (5) and (7) (see below) starting from Eq. (1) is deferred to Appendix A.

Now, to get rid of the CM momentum in Eq. (5), it is completely necessary to assume that the potential is of the form given by Eq. (4), i.e, a local potential not depending on the CM coordinate.[1] With this assumption, which is right for the kind of coarse-grained potential used in this work, one can obtain a similar equation to that given in (5) but for the relative ket, removing as much as possible the dependence on the CM momentum. The final result is

$$|\psi_{\mathbf{K}_{\rm CM},\mathbf{k}}\rangle = |\mathbf{k}\rangle + \int d^3k'\, \frac{Q(\mathbf{K}_{\rm CM},\mathbf{k}')}{k^2-k'^2}\,|\mathbf{k}'\rangle\langle\mathbf{k}'|2\mu V|\psi_{\mathbf{K}_{\rm CM},\mathbf{k}}\rangle, \tag{7}$$

where $|\psi_{\mathbf{K}_{\rm CM},\mathbf{k}}\rangle$ is the relative part of the perturbed $|\Psi_{\mathbf{K}_{\rm CM},\mathbf{k}}\rangle$ state of Eq. (5); $|\mathbf{k}\rangle$ is the plane wave state with definite relative momentum $\mathbf{k}$; and the integral over the off-shell states $|\mathbf{k}'\rangle$ now only runs over the relative two-nucleon momentum. It is not possible to remove completely all the dependence on the total momentum $\mathbf{K}_{\rm CM}$ because of the presence of the Pauli-blocking operator, as is obvious from Eq. (7).

[1]The assumption of locality is also exploited specifically in other computational frameworks such as the Monte Carlo approach [116–121]. As already mentioned in the introduction, the SRG method reduces the core at the expense of introducing strong nonlocalities. In contrast, the Monte Carlo method needs a strong repulsive core below 0.5 fm within a purely local interaction scheme. The main advantage of the coarse-graining approach is that the quality of the N-N interaction fits is compatible with the assumption that possible nonlocalities take place at distances below the coarse-graining scale of $\Delta r = 0.6$ fm, and *simultaneously* reduces the short distance core. As we will show, this has the further practical advantage of reducing tremendously the computational effort.

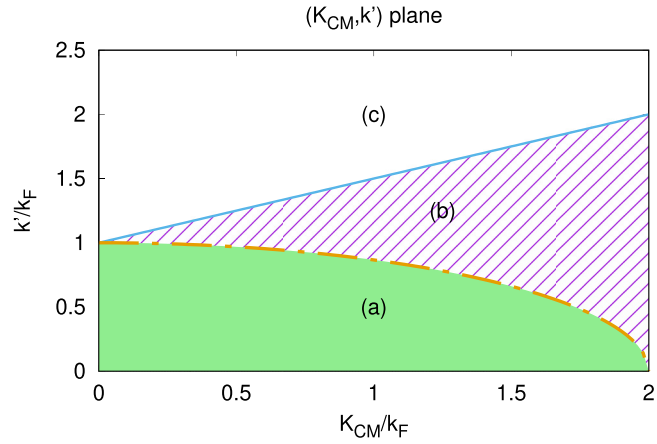

FIG. 1. Representation of the different zones of the phase space in the variables $(K_{\rm CM},k')$ where the angular average of the Pauli-blocking operator $\overline{Q}(K_{\rm CM},k')$ takes different values. To avoid specifying a definite value for the Fermi momentum k_F, the axes of the plot are represented in units of the Fermi momentum.

B. Angular average of the Pauli-blocking operator

The main problem when solving Eq. (7), besides the form of the N-N potential, is the additional angular dependence introduced by the Pauli-blocking function given in Eq. (6). Indeed, the function $Q(\mathbf{K}_{\rm CM},\mathbf{k}')$ depends explicitly on the polar angle between the vectors $\mathbf{K}_{\rm CM}$ and $\mathbf{k}'$ and, therefore, breaks rotational invariance in Eq. (7) even for a central N-N potential [127], causing a mixing among different partial waves if one tries to perform a partial wave expansion to solve Eq. (7). Although some few authors have solved the problem in general for different (noncentral) N-N potentials [128–133], we are going to use in this work the approximation, first proposed by Brueckner [9] and also taken by many other authors [36,108,109,124–126], of substituting the angle-dependent Pauli-blocking function $Q(\mathbf{K}_{\rm CM},\mathbf{k}')$ by its angular average around the direction defined by the CM momentum. This approximation amounts to performing the replacement

$$Q(\mathbf{K}_{\rm CM},\mathbf{k}') \longrightarrow \overline{Q}(K_{\rm CM},k') \equiv \frac{1}{4\pi}\int d\Omega_{\hat{k}'}\, Q(\mathbf{K}_{\rm CM},\mathbf{k}') \tag{8}$$

in Eq. (7). With this replacement, now the angle-averaged Pauli-blocking function $\overline{Q}(K_{\rm CM},k')$ only depends on the magnitude of both CM and relative momenta, but not on the angle between both vectors $(\widehat{\mathbf{K}_{\rm CM},\mathbf{k}'})$.

Obviously, the angular average of a function [see Eq. (6)] that can only take the values 1 or 0 is another function that can *continuously* reach values between 0 and 1 depending on the different zones of the $(K_{\rm CM},k')$ plane, as depicted in Fig. 1. The functional form of $\overline{Q}(K_{\rm CM},k')$ for $K_{\rm CM}<2\,k_F$ has been

well known since the time of Brueckner [9]:

$$\overline{Q}(K_{\rm CM},k') = \begin{cases} 0 & \text{if } 0 \leqslant k' \leqslant \sqrt{k_F^2-\frac{K_{\rm CM}^2}{4}}, \\ \frac{\frac{K_{\rm CM}^2}{4}+k'^2-k_F^2}{K_{\rm CM}\,k'} & \text{if } \sqrt{k_F^2-\frac{K_{\rm CM}^2}{4}} < k' \leqslant k_F+\frac{K_{\rm CM}}{2}, \\ 1 & \text{if } k' > k_F+\frac{K_{\rm CM}}{2}. \end{cases} \quad (9)$$

We restrict our study in this work to the zone $K_{\rm CM} < 2\,k_F$, corresponding to the abscissa axis range of Fig. 1, because this is the maximum total (CM) momentum of an uncorrelated nucleon pair in the ground state of nuclear matter, i.e., when both nucleons have their largest single momentum, k_F, in the parallel direction.

The region labeled by (a) in Fig. 1, where the angle-averaged Pauli-blocking function $\overline{Q}(K_{\rm CM},k')=0$, corresponds to the forbidden region for two nucleons to scatter below the Fermi momentum k_F; i.e., this region, limited by the quarter of an ellipse with semimajor and semiminor axes $2\,k_F$ and k_F, respectively, corresponds to the region where the single off-shell nucleon momenta satisfy that both $|\mathbf{k}_i'| < k_F$, and thus this region is excluded by the Pauli-blocking operator [cf. Eq. (2)].

The region labeled by (c) in Fig. 1, where the function $\overline{Q}(K_{\rm CM},k')$ takes the value 1, corresponds to the totally allowed region for two off-shell nucleons to scatter above the Fermi momentum k_F, i.e., this region bounded from below by the straight line $k'=k_F+\frac{K_{\rm CM}}{2}$ is the region where the single off-shell nucleon momenta always satisfy that both $|\mathbf{k}_i'| > k_F$, and thus this region is fully included by the Pauli-blocking operator [cf. Eq. (2)].

Finally, the region labeled by (b) in Fig. 1, bounded by the ellipse from below and by the straight line from above, corresponds to the transition region between both extreme situations of zones (a) and (c). In this region, (b), the angle-averaged Pauli-blocking function $\overline{Q}(K_{\rm CM},k')$ takes intermediate values between 0 and 1, depending of course on the values of $K_{\rm CM}$ and k' within this region. Physically, the picture of this region represents situations where, when performing the angular average of Eq. (8), for some values of the angle between $\mathbf{K}_{\rm CM}$ and $\mathbf{k}'$ both single nucleon momenta are above the Fermi momentum ($|\mathbf{k}_i'| > k_F$), thus contributing the maximum to the integral of Eq. (8); while for other values of the angle $(\widehat{\mathbf{K}_{\rm CM},\mathbf{k}'})$, one or both single momenta of the nucleon pair are below the Fermi momentum ($|\mathbf{k}_i'| < k_F$), thus contributing 0 to the integral. Therefore, the final result is an intermediate-valued function between 0 and 1, as shown in Fig. 2.

What is being shown in Fig. 2 is exactly the piecewise function $\overline{Q}(K_{\rm CM},k')$ of Eq. (9) when the momenta are expressed in units of the Fermi momentum k_F, for the same range in the variables $(\frac{K_{\rm CM}}{k_F},\frac{k'}{k_F})$ as that plotted in Fig. 1. Each panel corresponds to a selected value for the CM momentum of the nucleon pair, and the $\overline{Q}$ function is represented in terms of the relative momentum of the pair. We comment on several properties of this function:

(1) For $K_{\rm CM}=0$ the $\overline{Q}$ function is exactly a step function, namely $\theta(k'-k_F)$, and therefore it presents a discontinuity at the point $k'=k_F$. This situation corresponds to moving along the y axis in Fig. 1. In this case the function is zero on the green region until one reaches the point $k'=k_F$ (where the ellipse and the straight line cut each other), and beyond that point, for $k'>k_F$, the $\overline{Q}$ function is always equal to 1. Therefore, this corresponds to the situation when the region (b) of Fig. 1 reduces to a single point when moving along the y axis.

(2) For relatively low values of the CM momentum, $K_{\rm CM} \lesssim k_F$, the joining $\overline{Q}$ function between regions (a) and (c) of Fig. 1, i.e., along the region (b) of the same figure for a definite CM momentum (moving along a vertical straight line in Fig. 1), is almost a straight line with large slope. This is because the $\overline{Q}$ function has to increase from 0 to 1 in a relatively short range of k' values, thus making a larger slope.

(3) For intermediate values of the CM momentum, $k_F \lesssim K_{\rm CM} \lesssim 2\,k_F$, a clear curvature in the joining $\overline{Q}$ function is evident, especially at the lowest k' values, i.e., in region (b) of Fig. 1 but close to the ellipse. In addition, as the $\overline{Q}$ function has a longer range in k' values to rise from 0 to 1, the average slope is much less steep than in the case discussed in the previous point.

(4) For the maximum allowed CM momentum of two nucleons below the Fermi momentum, $K_{\rm CM}=2\,k_F$, the region (a) of Fig. 1 reduces to a single point ($k'=0$), and the $\overline{Q}$ function in region (b) of the same figure is exactly a straight line in the $\frac{k'}{k_F}$ variable with slope $\frac{1}{2}$. This can be analytically proved from the second line of Eq. (9) by simply substituting $K_{\rm CM}=2\,k_F$.

(5) Finally, it is worth noticing that, except for $K_{\rm CM}=0$, the piecewise function of Eq. (9) is a continuous function even at the curves separating the three different regions of Fig. 1, i.e., at the ellipse and the straight line of the same figure. However, this $\overline{Q}(K_{\rm CM},k')$ function has no continuous derivatives with respect to the k' variable precisely along the ellipse and the straight line of Fig. 1. This behavior is clearly observable from Fig. 2, where at the joining points where $\overline{Q}$ is 0 or 1, the slopes are different if one approaches that point from below or above it. This last behavior for the derivative at the curves delimiting the different regions in Fig. 1 was already pointed out in Ref. [108], and it will be very relevant to interpret the high-momentum components of the relative wave functions that will be shown in Sec. IV B.

C. B-G integral equation for the radial wave function

In principle, performing a partial wave expansion of Eq. (7) along the lines of that carried out in Ref. [9], a set of coupled integral equations is obtained for the radial components of the relative wave function. The formal derivation of this last equation is also deferred to Appendix B. In this work we extend the system of equations presented in [68]. This previous study considered these equations in the specific case

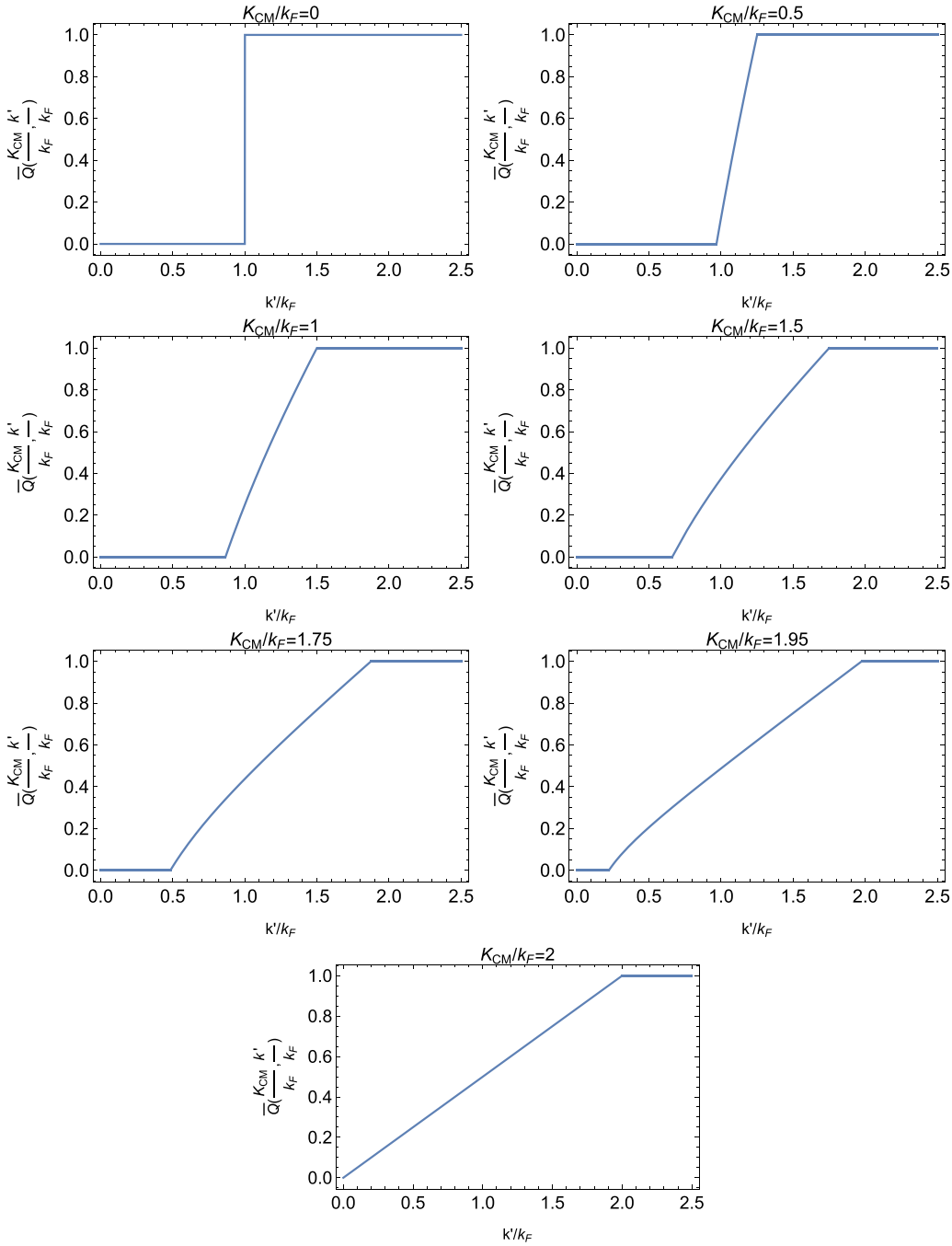

FIG. 2. Plots of the angle-averaged Pauli-blocking function $\overline{Q}(K_{\rm CM}, k')$ for different values of the total CM momentum of the nucleon pair, ranging from 0 up to $2\,k_F$. The different panels are labeled by the CM momentum in units of the Fermi momentum k_F. The abscissa axis corresponds to the relative k' momentum of the pair, in units of the Fermi momentum as well. The range spanned in the variables $(K_{\rm CM}, k')$ is the same as that also displayed in Fig. 1.

where the relative momentum is oriented along the z axis and the CM momentum is zero. However, in this paper we investigate the general case where the relative momentum can point in any direction, and the CM momentum is nonzero. This modification only impacts the radial functions in the coupled channels, which in Ref. [68] depended on a single angular momentum label, $\widetilde{u}_l$. In the general case considered here, these functions now depend on two angular momentum indices, $\widetilde{u}_{l\,l'}$. Another difference with respect to what was done in Ref. [68] is the form of the in-medium Green's function for the problem when $K_{\rm CM} \neq 0$.

Following the same normalization for the perturbed radial wave function as in Ref. [68], the result is

$$\widetilde{u}^{SJ}_{k,l\,l'}(r) = \hat{j}_l(kr)\delta_{ll'} + \int_0^\infty dr'\, \widetilde{G}^{K_{\rm CM}}_{k,l'}(r,r') \times \sum_{l''} U^{SJ}_{l',l''}(r')\, \widetilde{u}^{SJ}_{k,l\,l''}(r'), \tag{10}$$

where $\widetilde{u}^{SJ}_{k,l\,l'}(r)$ is the perturbed radial wave function; $\hat{j}_l(kr) = (kr)\,j_l(kr)$ is the reduced spherical Bessel function of the first kind; $U^{SJ}_{l,l'}(r) = 2\mu V^{SJ}_{l,l'}(r)$ is the reduced potential matrix element for the channel with total spin $S = 0, 1$ and total angular momentum J between partial waves with different (or equal) orbital angular momenta (l, l'); and, finally, $\widetilde{G}^{K_{\rm CM}}_{k,l}(r, r')$ is the Green's function for the radial B-G equation and it is given by

$$\widetilde{G}^{K_{\rm CM}}_{k,l}(r, r') = \frac{2}{\pi}\int_0^\infty dk'\,\hat{j}_l(k'r)\,\frac{\overline{Q}(K_{\rm CM}, k')}{k^2 - k'^2}\,\hat{j}_l(k'r'). \quad (11)$$

In general, the radial wave functions of Eq. (10) depend on two angular momentum indices, $\widetilde{u}_{l\,l'}$. Due to the tensor force, the channels with $l, l' = J \pm 1$ are coupled, while in the uncoupled channels one has $l = l'$ (see Appendix B).

Note that the radial wave functions $\widetilde{u}^{SJ}_{k,l\,l'}(r)$ also depend implicitly on the value of the CM momentum $K_{\rm CM}$, although this dependence has not been written explicitly in order to shorten the notation.

The Green's function of Eq. (11) is a symmetric function and reduces to the Green's function given in Eq. (13) of Ref. [68] for the particular case when $K_{\rm CM} = 0$. The integral of the oscillatory integrand of Eq. (11) over the infinite interval for $k' > k_F + \frac{K_{\rm CM}}{2}$ is carried out with Levin-type integration methods [136,137].

At first sight one could foresee a divergence in the integrand of Eq. (11) when $k' = k$. However, for the calculations carried out in this work, one should have in mind that the initial relative momentum k of the nucleon pair is restricted to lie in region (a) of Fig. 1, because only in this region do both initial nucleons have individual momenta below the Fermi momentum k_F. Despite the general limits of integration in Eq. (11), the averaged Pauli-blocking operator is zero unless $k' > \sqrt{k_F^2 - \frac{K_{\rm CM}^2}{4}}$. Therefore, the true lower limit in the integral of Eq. (11) is $k' = \sqrt{k_F^2 - \frac{K_{\rm CM}^2}{4}}$ instead of zero, for a general total momentum of the nucleon pair satisfying $K_{\rm CM} \leqslant 2k_F$. The only point where there could be some divergence in the integrand is when the initial relative momentum of the pair, k, lies exactly in the ellipse of Fig. 1. This would mean that there could be a singularity exactly at the truly initial point of the integration interval in Eq. (11). However, at this point, $k = k' = \sqrt{k_F^2 - \frac{K_{\rm CM}^2}{4}}$, the integrand is, in general, finite, as it can be proven below by taking the limit $k' \to k^+$. The only possible source of divergence is the quotient $\frac{\overline{Q}(K_{\rm CM}, k')}{k^2 - k'^2}$.

If we calculate the limit of this quotient when $k' \to k^+ \equiv \sqrt{k_F^2 - \frac{K_{\rm CM}^2}{4}}$, we obtain the result

$$\lim_{k'\to k^+}\frac{\overline{Q}(K_{\rm CM}, k')}{k^2 - k'^2} = \lim_{k'\to k^+}\frac{\frac{\frac{K_{\rm CM}^2}{4} + k'^2 - k_F^2}{K_{\rm CM}\,k'}}{k_F^2 - \frac{K_{\rm CM}^2}{4} - k'^2} = \lim_{k'\to k^+}\frac{-1}{K_{\rm CM}\,k'}.$$

Therefore, at the end, the only point of possible divergence corresponds to the case $K_{\rm CM} = 0$. In this particular case for the value of the total momentum of the nucleon pair, we are integrating over k' in Eq. (11) along the y axis of Fig. 1, and the only possible point of divergence corresponds to the case when $k = k' = k_F$. Note that in this case (see Fig. 1), the region (b) gets reduced to a single point where the averaged Pauli-blocking operator has a sudden discontinuity at $k' = k_F$, passing from zero to one, as the top left panel of Fig. 2 shows. In this case, effectively the integrand of Eq. (11) has a discontinuity, but only when the initial relative momentum k of the pair reaches its maximum allowed value k_F.

This situation physically corresponds to two back-to-back nucleons, each carrying the maximum single momentum k_F. In the calculations carried out here for $K_{\rm CM} = 0$, or in those performed in Ref. [68], we always have taken $k < k_F$, thus avoiding any problem related with this singularity.

Now, we can introduce in Eq. (10) the form of the coarse-grained Granada potential given by the sum of delta shells for each channel, defined by the values of the total spin S and total angular momentum J:

$$U^{SJ}_{l,l'}(r) = \sum_{i=1}^{N_\delta}(\lambda_i)^{SJ}_{l,l'}\,\delta(r - r_i), \quad (12)$$

where the five ($N_\delta = 5$) delta-shells strengths $(\lambda_i)^{SJ}_{l,l'}$ are given in Table I of Ref. [123], and they were fitted to reproduce the phase shifts of N-N scattering below the pion production threshold. In this calculation we neglect the one-pion exchange (OPE) contribution, which starts at distances larger than 3 fm. While this contribution is essential to describe the physical scattering data with a high quality fit (particularly for the peripheral waves), its influence becomes marginal for the study of short distance correlations and makes the calculation unnecessarily more cumbersome.

The whole point of our framework has been to realize in previous works that, even though in the current and traditional jargon of nuclear physics, short distance effects are thought to imply extremely small wavelengths, this is actually not so. Including more delta shells does not improve the description of the scattering data in the elastic regime. In fact, from a statistical point of view, the fits to the N-N data do not improve but the statistical correlation among fitting parameters increases and, hence, these additional deltas are largely redundant.

At the present stage it is difficult to ponder on the impact on 3,4,5-body excitations within our approach. There have been attempts where mostly the 3-body interaction is included [138–143] as an effective (averaged) 2-body one. Our expectation would be that these terms may modify the total strength of the wave function but not the asymptotic behavior.

With this kind of potential given in Eq. (12), one can easily perform the integral over the radial coordinate in Eq. (10), thus obtaining the following algebraic equation

$$\widetilde{u}^{SJ}_{k,l\,l'}(r) = \hat{j}_l(kr)\delta_{ll'} + \sum_{i=1}^{N_\delta}\widetilde{G}^{K_{\rm CM}}_{k,l'}(r, r_i)\sum_{l''}(\lambda_i)^{SJ}_{l',l''}\,\widetilde{u}^{SJ}_{k,l\,l''}(r_i). \quad (13)$$

The form of the potential, Eq. (12), has allowed us to transform, in general, a coupled integral equation for the radial wave functions, Eq. (10), into a linear system of coupled algebraic equations for the radial wave functions *at the grid points* r_i. Indeed, if we now take $r = r_j$ with $j = 1, 2, \ldots, N_\delta$, then Eq. (13) transforms into the coupled linear system

given by

$$\widetilde{u}^{SJ}_{k,l\,l'}(r_j) = \hat{j}_l(kr_j)\delta_{ll'} + \sum_{i=1}^{N_\delta} \widetilde{G}^{K_{\rm CM}}_{k,l'}(r_j, r_i) \times \sum_{l''} (\lambda_i)^{SJ}_{l',l''}\, \widetilde{u}^{SJ}_{k,l\,l''}(r_i). \tag{14}$$

Once the values of the radial wave functions at the grid points are obtained, the B-G equation itself, namely Eq. (13), directly allows for a sensible interpolation of the wave function to any point between the grid points.

The total spin S of the two-nucleon system is known to be conserved by the N-N interaction. When the two nucleons are in a singlet spin state, $S = 0$, then the tensor force does not couple states with different orbital angular momentum, and therefore $l = l' = l'' = J$ in Eq. (14). In this case we have an inhomogeneous linear system of $N_\delta = 5$ equations (one for each one of the possible values of r_j) with five unknowns, which are the five values of the radial wave functions $\widetilde{u}^{0J}_{k,J}(r_i)$ at the five grid points r_i.

When the two nucleons are coupled to total spin $S = 1$, for a given total angular momentum J of the partial wave, there are three possibilities for the orbital angular momentum, $l = J-1, J, J+1$, except for $J = 0$, where only $l = 1$ (P state) is allowed. Due to the conservation of parity in the N-N interaction, in the triplet channels ($S = 1$), partial waves with angular momenta $l = l' = J$ and parity $P = (-1)^J$ are decoupled from those with $l, l' = J \pm 1$ and parity $P = (-1)^{J+1}$. In the former case, $l = l' = J$, Eq. (14) reduces again to five equations for the radial wave function values at the grid points.

However, the partial waves for the case $S = 1$ and $(l, l') = J-1, J+1$ are known to be coupled due to the tensor part of the N-N interaction, which has off-diagonal components in the orbital angular momentum basis. In this case, we have to simultaneously solve a coupled system for four different radial wave functions at the grid points of the form given in Eq. (14). Now the sum over l'' in Eq. (14) runs over two values $l'' = J-1, J+1$ for each pair of (l, l') values. Therefore, the linear system we have to solve in this case is, *a priori*, a coupled inhomogeneous one of 20 equations with 20 unknowns. These unknowns are precisely the four coupled radial wave functions at the five grid points.

Finally, once the values of the perturbed radial wave function for each partial wave $^{2S+1}l_J$ are known at the grid points, $\widetilde{u}^{SJ}_{k,l\,l'}(r_i)$, then the wave function can be known at any other point r by means of Eq. (13).

Just to see the difference with respect to Eqs. (16) and (17) of Ref. [68], which are valid only when the relative momentum $\mathbf{k}$ defines the z axis, we write below the general coupled equations for the $^3S_1$ - $^3D_1$ coupled channels:

$$\widetilde{u}^{11}_{k,00}(r) = \hat{j}_0(kr) + \int_0^\infty dr'\, \widetilde{G}^{K_{\rm CM}}_{k,0}(r, r')\big[U^{11}_{0,0}(r')\, \widetilde{u}^{11}_{k,00}(r') + U^{11}_{0,2}(r')\, \widetilde{u}^{11}_{k,02}(r')\big], \tag{15}$$

$$\widetilde{u}^{11}_{k,02}(r) = \int_0^\infty dr'\, \widetilde{G}^{K_{\rm CM}}_{k,2}(r, r')\big[U^{11}_{2,0}(r')\, \widetilde{u}^{11}_{k,00}(r') + U^{11}_{2,2}(r')\, \widetilde{u}^{11}_{k,02}(r')\big], \tag{16}$$

$$\widetilde{u}^{11}_{k,20}(r) = \int_0^\infty dr'\, \widetilde{G}^{K_{\rm CM}}_{k,0}(r, r')\big[U^{11}_{0,0}(r')\, \widetilde{u}^{11}_{k,20}(r') + U^{11}_{0,2}(r')\, \widetilde{u}^{11}_{k,22}(r')\big], \tag{17}$$

$$\widetilde{u}^{11}_{k,22}(r) = \hat{j}_2(kr) + \int_0^\infty dr'\, \widetilde{G}^{K_{\rm CM}}_{k,2}(r, r')\big[U^{11}_{2,0}(r')\, \widetilde{u}^{11}_{k,20}(r') + U^{11}_{2,2}(r')\, \widetilde{u}^{11}_{k,22}(r')\big]. \tag{18}$$

Note that Eqs. (15) and (16) involve only the components $(l, l') = (00), (02)$ of the radial wave functions, while Eqs. (17) and (18) involve $(l, l') = (20), (22)$. Therefore, these two pairs of equations can be solved separately as two linear systems of ten equations with ten unknowns when using the coarse-grained potential with five delta shells.

III. RELATIVE WAVE FUNCTION IN MOMENTUM SPACE

The derivation of the results of this section follows almost the same lines as those of Sec. III C of Ref. [68], with caution because in general the perturbed radial wave functions depend now on two angular momentum labels, $l\,l'$ (as sketched in Sec. II C and shown in Appendix B), but for the general case when $K_{\rm CM} \neq 0$. At the end of Sec. II A we wrote the B-G equation that satisfies the relative perturbed wave function $|\psi_{\mathbf{K}_{\rm CM},\mathbf{k}}\rangle$ without mentioning the spin of the two-nucleon pair; cf. Eq. (7). When the approximation of performing the angular average of the Pauli-blocking operator is taken into account, the relative ket $|\psi_{\mathbf{K}_{\rm CM},\mathbf{k}}\rangle$ no longer depends on the direction of the CM momentum $\hat{K}_{\rm CM}$ of the two-nucleon system; i.e., all directions of the CM momentum are equivalent in infinite nuclear matter. Or, to say it in other words, there is an isotropy property for the direction of the CM momentum $\hat{K}_{\rm CM}$.

If, finally, we also add the spin state of the two-nucleon pair to the relative ket state we have a new ket state, labeled as $|\psi_{\mathbf{k}}, SM_S\rangle_{K_{\rm CM}}$, whose meaning is that it is the perturbed ket state with initial unperturbed relative momentum $\mathbf{k}$ of the two-nucleon system, and with total spin S and third component of spin M_S. This relative ket state can be projected over the bra $\langle\mathbf{p}|$ to obtain the probability amplitude of finding the state $|\psi_{\mathbf{k}}, SM_S\rangle_{K_{\rm CM}}$ in other one with relative momentum $\mathbf{p}$ due to the N-N interaction and the medium (angular average of the Pauli-blocking operator) effects.

If we had an unperturbed state with relative momentum $\mathbf{k}$ and spin state (S, M_S), its wave function in coordinate representation would be

$$\begin{aligned}\langle\mathbf{r}|\mathbf{k}; SM_S\rangle &= \frac{e^{i\,\mathbf{k}\cdot\mathbf{r}}}{(2\pi)^{\frac{3}{2}}}\, \chi_{SM_S} \\ &= \frac{4\pi}{(2\pi)^{\frac{3}{2}}} \sum_{J,M} \sum_{l,m} i^l\, j_l(kr)\, Y^*_{lm}(\hat{k}) \langle lm; SM_S|JM\rangle \\ &\quad \times \mathcal{Y}_{lSJM}(\hat{r}) \\ &= \frac{4\pi}{(2\pi)^{\frac{3}{2}}} \sum_{J,M} \sum_{l,l',m} i^l\, j_l(kr)\, Y^*_{l'm}(\hat{k})\, \delta_{l'l} \\ &\quad \times \langle l'm; SM_S|JM\rangle\, \mathcal{Y}_{lSJM}(\hat{r}),\end{aligned} \tag{19}$$

where in the last step we have added an additional sum over l' with the Kronecker delta $\delta_{l'l}$ in order to match the expansion of the perturbed or correlated state (see below).

In Eq. (19) we have coupled the orbital angular momentum and spin angular momentum states, i.e., $l \otimes S$, to obtain the spin-angular eigenfunctions, $\mathcal{Y}_{lSJM}(\hat{r})$, with well-defined total angular momentum J and third component M, defined by

$$\mathcal{Y}_{lSJM}(\hat{r}) = \sum_{m,M_S} \langle lm; SM_S|JM\rangle Y_{lm}(\hat{r})\ \chi_{sM_S}. \tag{20}$$

A similar expansion in partial waves to that of Eq. (19) also holds for the perturbed state $|\psi_{\mathbf{k}}, SM_S\rangle_{K_{\rm CM}}$ in coordinate representation,

$$\langle \mathbf{r}\,|\psi_{\mathbf{k}}, SM_S\rangle_{K_{\rm CM}} = \frac{4\pi}{(2\pi)^{\frac{3}{2}}} \sum_{J,M} \sum_{l,l',m} i^{l'}\, Y^*_{l'm}(\hat{k})\ u^{SJ}_{k,l'l}(r) \times \langle l'm; SM_S|JM\rangle\ \mathcal{Y}_{lSJM}(\hat{r}), \tag{21}$$

where the perturbed radial wave functions $u^{SJ}_{k,l'l}(r)$ are normalized with respect to those appearing in Sec. II C as

$$u^{SJ}_{k,l'l}(r) = \frac{\widetilde{u}^{SJ}_{k,l'l}(r)}{k\,r}, \tag{22}$$

in order to approach the free solution, the spherical Bessel functions of the first kind, at long distances for the diagonal case, $l = l'$.

With these two partial wave expansions for the unperturbed and perturbed states, Eqs. (19) and (21), we can calculate the bra-ket product $\langle \mathbf{p}|\psi_{\mathbf{k}}, SM_S\rangle_{K_{\rm CM}}$ in momentum space by performing the Fourier transform:

$$\begin{aligned}\langle \mathbf{p}|\psi_{\mathbf{k}}, SM_S\rangle_{K_{\rm CM}} &= \int \frac{d^3r}{(2\pi)^{\frac{3}{2}}} e^{-i\,\mathbf{p}\cdot\mathbf{r}} \langle \mathbf{r}|\psi_{\mathbf{k}}, SM_S\rangle_{K_{\rm CM}} \\ &= \frac{2}{\pi} \sum_{J,M} \sum_{l,l',m} i^{l'-l}\, Y^*_{l'm}(\hat{k}) \langle l'm; SM_S|JM\rangle \\ &\quad \times \mathcal{Y}_{lSJM}(\hat{p}) \frac{1}{p\,k} \int_0^\infty dr\ \hat{j}_l(pr)\ \widetilde{u}^{SJ}_{k,l'l}(r).\end{aligned} \tag{23}$$

To obtain the final expression of Eq. (23), we have used the expansion of the plane wave in spherical harmonics (Rayleigh's formula) and Eq. (21) for the perturbed wave function in coordinate representation, and we have also carried out the angular integration over $\hat{r}$ between a spherical harmonic and a spin-angular eigenfunction, with the aid of

$$\int d\Omega_{\hat{r}}\ Y^*_{l'm'}(\hat{r})\ \mathcal{Y}_{lSJM}(\hat{r}) = \delta_{l,l'} \sum_{m_s} \langle lm'; Sm_s|JM\rangle\ \chi_{Sm_s}. \tag{24}$$

Finally, we have performed the sum over the orbital angular momentum label with the Kronecker delta, and we have coupled again one spherical harmonic with the spinor wave function appearing in Eq. (24) to obtain the spin-angular eigenfunction $\mathcal{Y}_{lSJM}(\hat{p})$.

The form of Eq. (23), apart from the normalization factors, is completely equivalent to that of the perturbed ket in position representation, given by Eq. (21). In this case, we identify the "radial" partial wave function in momentum representation as

$$\phi^{SJ}_{k,l'l}(p) = \frac{2}{\pi} \frac{1}{p\,k} \int_0^\infty dr\ \hat{j}_l(pr)\ \widetilde{u}^{SJ}_{k,l'l}(r). \tag{25}$$

It is also worth noticing that the "radial" wave function $\phi^{SJ}_{k,l'l}(p)$ for each partial wave also depends on the magnitude of the CM momentum of the nucleon pair, $K_{\rm CM}$, via the dependence on it of the radial wave function $\widetilde{u}^{SJ}_{k,l'l}(r)$ [cf. Eq. (13)], as already been mentioned in the discussion given in Sec. II C. However, this dependence has not been explicitly written here to avoid a very cumbersome notation.

In the next step, to obtain an analytical expression for the "radial" wave function $\phi^{SJ}_{k,l'l}(p)$, one needs to substitute the radial wave function $\widetilde{u}^{SJ}_{k,l'l}(r)$ from Eq. (13) into Eq. (25), and to use the explicit expression of the Green's function, $\widetilde{G}^{K_{\rm CM}}_{k,l}(r, r')$, given in Eq. (11), to carry out the integration over the radial variable in Eq. (25). It is also necessary to use the orthogonality property of the reduced spherical Bessel functions,

$$\int_0^\infty dr\ \hat{j}_l(pr)\ \hat{j}_l(kr) = \frac{\pi}{2}\ \delta(p-k), \tag{26}$$

to obtain the final result:

$$\phi^{SJ}_{k,l'l}(p) = \delta_{l'l} \frac{1}{p\,k}\ \delta(p-k) + \Delta\phi^{SJ}_{k,l'l}(p), \tag{27}$$

where

$$\Delta\phi^{SJ}_{k,l'l}(p) = \frac{2}{\pi} \frac{1}{p\,k} \frac{\overline{Q}(K_{\rm CM}, p)}{k^2 - p^2} \sum_{i=1}^{N_\delta} \hat{j}_l(pr_i) \times \sum_{l''} (\lambda_i)^{SJ}_{l,l''}\ \widetilde{u}^{SJ}_{k,l'l''}(r_i). \tag{28}$$

The first term of Eq. (27) corresponds to the unperturbed "radial" component of the state $|\psi_{\mathbf{K}_{\rm CM},\mathbf{k}}\rangle$ of Eq. (7), coming from the bra-ket product $\langle \mathbf{p}|\mathbf{k}\rangle$, while the second term, given explicitly in Eq. (28), corresponds actually to the high momentum components induced in the perturbed relative wave function by the N-N interaction and the medium.

For the ground state of an uncorrelated two-nucleon system in nuclear matter with single momenta $|\mathbf{k}_i| \leqslant k_F$, their relative momentum k is constrained to lie in region (a) of Fig. 1. Therefore, there is no divergence problem in the second term of Eq. (27) when p approaches k from above, because in that case the angle-averaged Pauli-blocking function $\overline{Q}(K_{\rm CM}, p)$ is exactly 0 on the ellipse delimiting region (a) from (b) in Fig. 1, and below the ellipse as well [cf. Eq. (9)].

Another interesting check corresponds to the case when the CM momentum of the two-nucleon system is zero, $K_{\rm CM} = 0$. In this case, Eq. (28) should reduce to Eq. (30) of Ref. [68]. And indeed this is the case, because for $K_{\rm CM} = 0$ the angle-averaged Pauli-blocking function $\overline{Q}(0, p)$ reduces to the step function $\theta(p - k_F)$, as can be deduced from the discussion given in point 1 of Sec. II B.

Some words of caution must be given again: in general, the radial wave functions, either in coordinate or momentum representation, depend on two labels for the orbital angular momenta, except for the uncoupled nucleon-nucleon partial

waves, where $l = l'$ and there are no off-diagonal wave functions.

A. High-momentum density distribution

We are going to obtain the high-momentum density distributions for a given total spin $S = 0, 1$ of the nucleon pair. To this end, we have to integrate the modulus squared of the *probability amplitude*, given in Eq. (23), of finding the perturbed wave function with momentum $\mathbf{p}$, over the solid angle of $\hat{p}$, assuming that we do not measure the direction of this momentum with respect to the fixed CM momentum, $\mathbf{K}_{\rm CM}$. This quantity is given by

$$\begin{aligned}\rho^{SM_S}_{\mathbf{k},K_{\rm CM}}(p) &= \int d\Omega_{\hat{p}} |\langle \mathbf{p}|\psi_{\mathbf{k}}, SM_S\rangle_{K_{\rm CM}}|^2 \\ &= \sum_{l,l',m}\sum_{l'',m''}\sum_{JM} i^{l'-l''}\, Y^*_{l'm}(\hat{k})\, Y_{l''m''}(\hat{k}) \\ &\quad \times \langle l'm; SM_S|JM\rangle \langle l''m''; SM_S|JM\rangle \phi^{SJ*}_{k,l''l}(p) \\ &\quad \times \phi^{SJ}_{k,l'l}(p), \end{aligned} \tag{29}$$

where we have used the orthogonality property of the spin-angular eigenfunctions $\mathcal{Y}_{lSJM}(\hat{p})$ to integrate over the directions of $\hat{p}$,

$$\int d\Omega_{\hat{p}}\, \mathcal{Y}^*_{l'SJ'M'}(\hat{p})\, \mathcal{Y}_{lSJM}(\hat{p}) = \delta_{l,l'}\, \delta_{J,J'}\, \delta_{M,M'}, \tag{30}$$

to carry out some discrete sums appearing when taking the modulus squared of Eq. (23).

If, in addition, we do not measure the third component of the spin of the pair of nucleons along the quantization axis defined by $\mathbf{K}_{\rm CM}$, we have to perform again a sum over M_S in Eq. (29), and an average over the number of different M_S values for each total spin S. We thus obtain

$$\begin{aligned}\rho^{S}_{\mathbf{k},K_{\rm CM}}(p) &= \frac{1}{2S+1}\sum_{M_S=-S}^{S} \rho^{SM_S}_{\mathbf{k},K_{\rm CM}}(p) \\ &= \frac{1}{2S+1}\sum_{l,l',m}\sum_{l'',m''}\sum_{J} i^{l'-l''}\, Y^*_{l'm}(\hat{k})\, Y_{l''m''}(\hat{k}) \\ &\quad \times \phi^{SJ*}_{k,l''l}(p)\, \phi^{SJ}_{k,l'l}(p) \sum_{M,M_S} \langle l'm; SM_S|JM\rangle \\ &\quad \times \langle l''m''; SM_S|JM\rangle. \end{aligned} \tag{31}$$

Note that the final sum over the third components of angular momenta of the product of two Clebsch-Gordan (C-G) coefficients can be carried out with the aid of the symmetry properties of these coefficients when changing the order of coupling, and using their orthonormality properties. The symmetry property that we need here is to change the order of coupling from $[l \otimes S]_J$ to $[J \otimes S]_l$, where l stands for anyone of the two orbital angular momenta appearing in Eq. (31):

$$\langle lm; SM_S|JM\rangle = (-1)^{S+M_S}\sqrt{\frac{2J+1}{2l+1}}\langle J, -M; SM_S|\, l, -m\rangle. \tag{32}$$

Using the above symmetry property of the C-G coefficients in the last sum of Eq. (31), we obtain

$$\begin{aligned}\rho^{S}_{\mathbf{k},K_{\rm CM}}(p) &= \frac{1}{2S+1}\sum_{l,l',m}\sum_{J} Y^*_{l'm}(\hat{k})\, Y_{l'm}(\hat{k})\, \Delta(JSl') \\ &\quad \times \frac{(2J+1)}{(2l'+1)}\, \left|\phi^{SJ}_{k,l'l}(p)\right|^2. \end{aligned} \tag{33}$$

To obtain the above equation we have used the following in the final sum of Eq. (31) over the third components M, M_S: the fact that the factor $(-1)^{2(S+M_S)}$ is always positive regardless of the spin of the nucleon pair being integer or half-integer (of course it is always integer, but the factor would also be positive in the case of half-integer spin); the fact that the sum over $M \equiv -M'$ can be carried out in reverse order without changing anything; the orthonormality property of the C-G coefficients, which when summed over M, M_S give $\Delta(JSl')\, \delta_{l',l''}\, \delta_{m,m''}$; and, finally, performing the sums over l'' and m'' with the aid of the Kronecker deltas.

Finally, notice that in Eq. (33) the sum over m only affects the spherical harmonics, and this can be simplified a lot by using

$$\sum_{m} Y^*_{l'm}(\hat{k})\, Y_{l'm}(\hat{k}) = \frac{(2l'+1)}{4\pi}, \tag{34}$$

thus giving the final result

$$\rho^{S}_{k,K_{\rm CM}}(p) = \frac{1}{2S+1}\sum_{l,l',J}\Delta(JSl')\, \frac{(2J+1)}{4\pi}\, \left|\phi^{SJ}_{k,l'l}(p)\right|^2. \tag{35}$$

It is also worth noting that $\Delta(JSl')$ is the triangular inequality for the coupling of two angular momenta to a third one, meaning that the sum over J and l' in Eq. (35) is restricted to run over those values of J and l' that are compatible for coupling to a total spin of the two-nucleon system of $S = 0$ or $S = 1$. To be more specific, for a given total spin S and total angular momentum J for the partial wave, the sum over l' runs from $|J - S|$ to $J + S$, with another restriction coming from the antisymmetry of the relative wave function for a system of two identical fermions such as the proton-proton (pp) or neutron-neutron (nn) pair. For these cases, if $S = 0$ (antisymmetric spin state in terms of the single nucleon spin states) then only even orbital angular momenta contribute; while if $S = 1$ (symmetric spin state in terms of the single nucleon spin states) only odd values of l and l' contribute in the sum of Eq. (35). However, this is not the case for a neutron-proton (np) pair, where all the (l, l') values compatible with the rules of angular momentum coupling (from $|J - S|$ to $J + S$), and coupling of partial waves due to the tensor force of the N-N potential are allowed in the sum of Eq. (35).

Finally, it is also worth warning the reader that Eq. (35) is the general equation instead of Eq. (34) of Ref. [68], where the relative momentum $\mathbf{k}$ was chosen to lie along the z axis. Although not explicitly written, the "radial" momentum wave functions $\phi^{SJ}_{k,l'l}(p)$ depend on the magnitude of the CM momentum of the two-nucleon system, while in Ref. [68] the results were obtained for $K_{\rm CM} = 0$ only. However, in order to facilitate the comparisons with the results of Ref. [68] for the high-momentum density distributions for a given total spin S

of the nucleon pair, and to see the differences, in the results section (Sec. IV) we are going to use the same normalization for the high-momentum density distributions as defined in Ref. [68], i.e., we are going to adopt the convention of Eq. (43) of that reference to plot the high-momentum density distributions for a given spin S. This convention amounts to plot $4\pi(2S+1)\rho^S_{k,K_{\rm CM}}(p)$, with $\rho^S_{k,K_{\rm CM}}(p)$ defined by Eq. (35), in order for a straightforward comparison of Figs. 8, 9(a), and 10 of Ref. [68] with the ones obtained from Eq. (35) (see Sec. IV for the discussion).

IV. RESULTS AND DISCUSSION

In this section we provide results for the perturbed radial wave functions in coordinate and momentum representations. We show the results for a Fermi momentum of $k_F = 250$ MeV/c and an initial relative momentum of the pair of $k = 140$ MeV/c, in order to compare with what was done in Ref. [68]. The results of this section were calculated for different CM momenta. All the pairs $(K_{\rm CM}, k)$ belong to the region (a) of Fig. 1, thus we are always in the region where the single-nucleon momenta are below the Fermi momentum ($|\mathbf{k}_i| \leqslant k_F$), i.e., in the ground state of nuclear matter.

While we show for definiteness results for $k = 140$ MeV/c of relative momentum, halfway to the Fermi momentum, we have verified that our conclusions regarding the CM do not depend strongly on the particular k value. Actually, for zero CM momentum, the universality of the particle pair distribution was explicitly verified in our previous work for $k = 40, 140, 200$ MeV/c (see Fig. 10(a) in Ref. [68]). However, the wave function with initial momentum k does depend directly on the CM momentum as a direct consequence of the B-G equation, as can be seen explicitly in Eq. (28). Regarding the Fermi momentum dependence, as a direct consequence of the Pauli blocking kernel, the momentum distribution is shifted above the Fermi momentum.

A. Perturbed radial wave functions in coordinate representation

In this subsection, for the uncoupled partial waves, $l = l'$, we use the notation $\widetilde{u}^{SJ}_{k,l} \equiv \widetilde{u}^{SJ}_{k,l\,l}$ for the radial wave functions in the figures.

In Fig. 3 we show results for the radial wave functions in coordinate representation, corresponding to the solutions of Eq. (13) for the uncoupled N-N partial waves for different total CM momenta of the nucleon pair corresponding to $K_{\rm CM} = 0,\ 100,\ 200,\ 300$, and 400 MeV/$c$. All these CM momenta are compatible with having a relative momentum of the nucleon pair $k = 140$ MeV/c and both initial single-nucleon momenta fulfilling the condition of lying below the Fermi momentum k_F (in fact, the maximum allowed CM momentum for $k = 140$ MeV/c under the above conditions corresponds to $K^{\rm max}_{\rm CM} = 414.25$ MeV/c). The values of the strength parameters $(\lambda_i)^{SJ}_{l,l'}$ of the delta-shell Granada potential are those of Table I of Ref. [123] and they were fitted to reproduce the N-N scattering phase-shifts of the Granada database [144] below the pion production threshold.

It is evident from Fig. 3 that the impact of the two-nucleon CM motion on the radial wave functions is minimal within the scale of the figure. However, it becomes more noticeable for the low-lying uncoupled partial waves, such as the S or P waves. For the D waves, the effect is a bit more pronounced in the triplet $^3D_2$ partial wave than in the singlet $^1D_2$ one, because of the strength parameters of the potential at the first delta shell (in this case they correspond to λ_2 in Table I of [123]); the attractive behavior of the first delta-shell parameter in the $^3D_2$ partial wave is much stronger than in the $^1D_2$ one.

The reasons for the SRCs' effects (distortions in the radial wave functions) being more distinguishable in the low lying l partial waves have to do not only with the strength parameters of the delta-shell potential (cf. Table I of Ref. [123]), but also with the centrifugal barrier of each partial wave (rising with the l value), which prevents the two nucleons from approaching each other more closely. The effects of SRCs are particularly noticeable at short internucleon distances. In the case of higher partial waves, such as D or F waves, the probability of nucleons approaching each other is significantly suppressed due to the presence of the centrifugal barrier. As a result, the influence of SRCs on these higher partial waves is less pronounced compared to the lower ones.

Nonetheless, the important point of Fig. 3 is that there is little dependence on the CM momentum in the perturbed radial wave functions at short distances, and this fact will have important consequences in the momentum distributions for each partial wave, $\Delta\phi^{SJ}_{k,l'l}(p)$ [Eq. (28)], at high probed relative momenta p, as will be shown later.

In order to magnify the differences between the perturbed wave functions and the free ones shown in Fig. 3, we present the defect wave functions in Fig. 4. These are defined as the difference between the perturbed wave functions and the free solutions,

$$\Delta\widetilde{u}^{SJ}_{k,l}(r) \equiv \widetilde{u}^{SJ}_{k,l}(r) - \hat{j}_l(kr), \tag{36}$$

for the diagonal $l' = l$ case.

Here we also observe the general trend discussed in Fig. 3, namely, the amplitude of the distortion in the perturbed wave function (importance of SRCs effects), in general, gets smaller when the value of the orbital angular momentum l increases (cf. the different scales in the vertical axes of Fig. 4), thus reflecting the importance of the centrifugal barrier that prevents the two nucleons from approaching each other more closely and experiencing the short-range N-N interaction, although the strength parameters of the delta-shell Granada potential also play a role. On the other hand, the magnitude of the distortion is quite insensitive to the state of global motion of the two-nucleon system, i.e., the value of the CM momentum (notice that the values at the cusps are more or less the same for the different curves in each panel of Fig. 4). Therefore, we can write, in general, a sort of hierarchy for the magnitude of the distortions in the wave functions due to the SRCs:

$$\Delta\widetilde{u}_{l=0} > \Delta\widetilde{u}_{l=1} > \Delta\widetilde{u}_{l=2} > \Delta\widetilde{u}_{l=3}. \tag{37}$$

It is also worth noticing that the amplitudes of the distortions in Fig. 4 are related to the importance of that partial wave in the two-nucleon relative high-momentum distribution

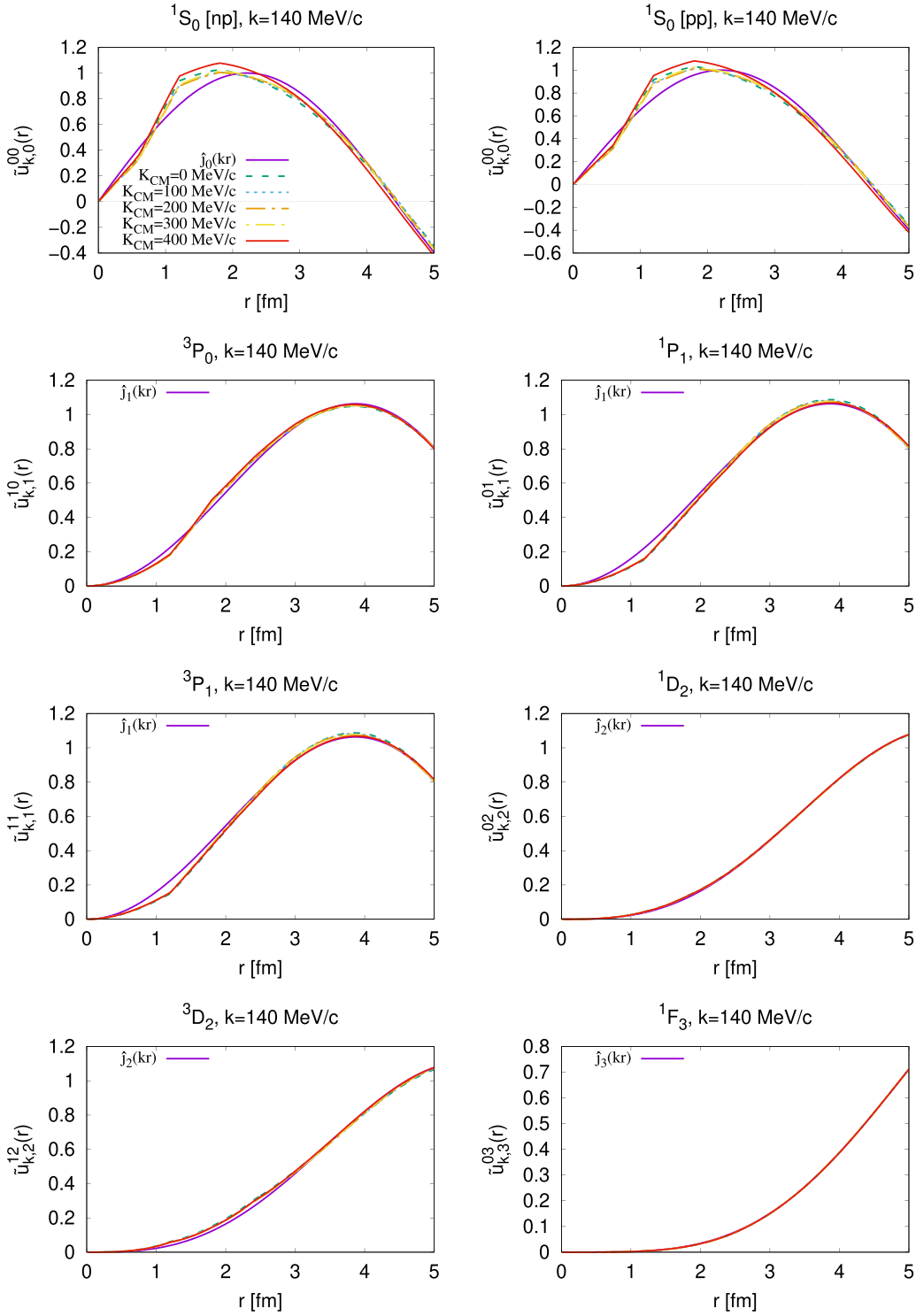

FIG. 3. Reduced radial wave functions $\tilde{u}^{SJ}_{k,l}(r)$ for the uncoupled N-N partial waves ($l = l'$). The results are given for relative momentum $k = 140$ MeV/c, and for each partial wave the free solution $\hat{j}_l(kr)$ as well as those for different values of the CM momentum are given. The results for $K_{\rm CM} = 0$ MeV/c (dashed green lines) are the same as those shown in Fig. 1 of Ref. [68]. Although not distinguishable in all panels, the curves labeled in the key of the $^1S_0[np]$ panel are also displayed in all the others.

$\rho^S_{k,K_{\rm CM}}(p)$ given by Eq. (35), since the different wavelengths overlapping (with different amplitudes of course) in the defect wave functions of the same figure are related to the corresponding high-momentum components in the relative momentum distribution for each partial wave $|\phi^{SJ}_{k,l'l}(p)|^2$, as in any continuous harmonic Fourier analysis.

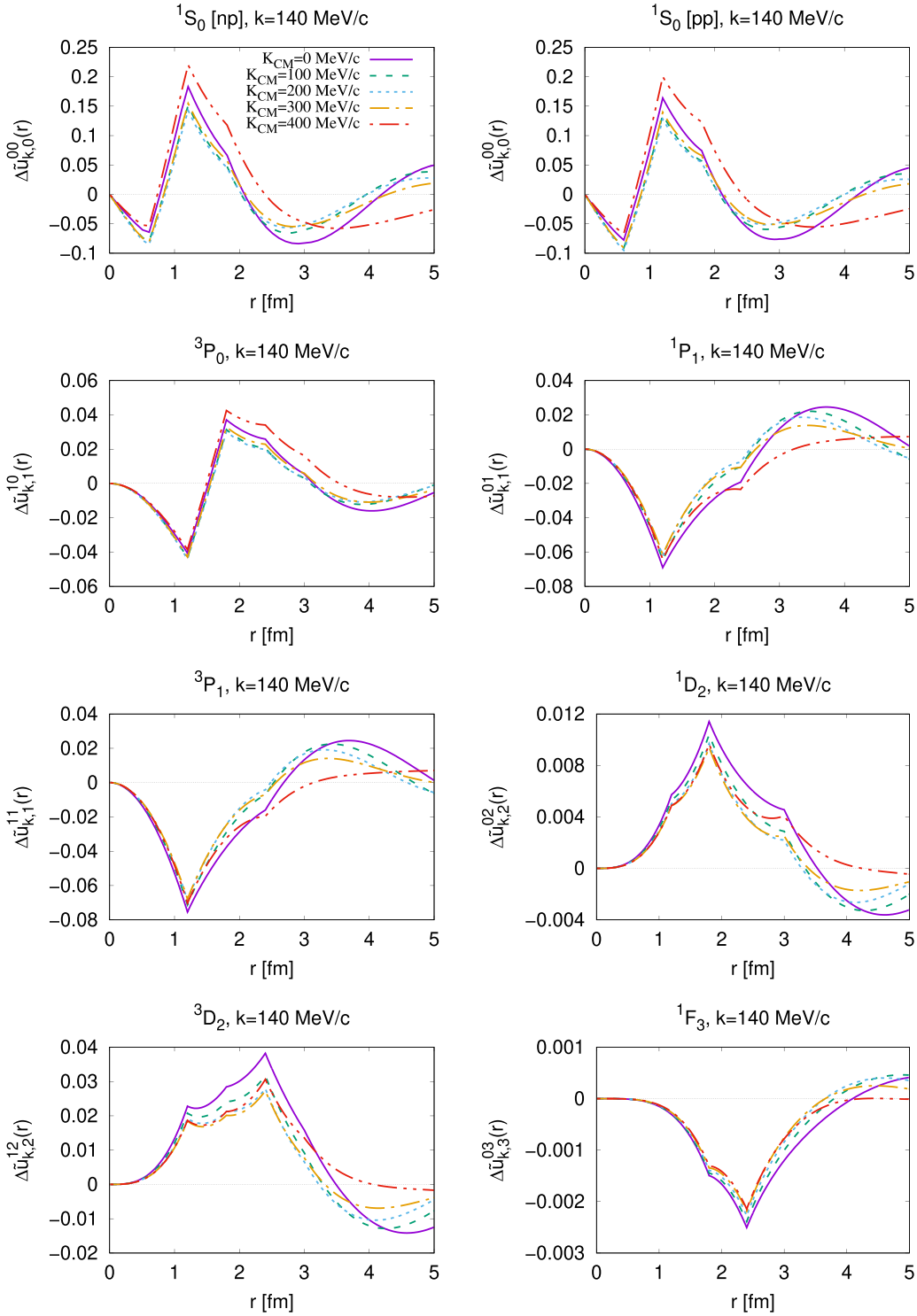

FIG. 4. Defect wave functions $\Delta\widetilde{u}^{SJ}_{k,l}(r) \equiv \widetilde{u}^{SJ}_{k,l}(r) - \hat{j}_l(kr)$ for the uncoupled N-N partial waves, $l' = l$. The results are given for relative momentum $k = 140$ MeV/c and for the same values of the CM momentum as in Fig. 3. The results for $K_{\rm CM} = 0$ MeV/c (solid purple lines) are the same as those shown as short-dashed green lines in Fig. 1 of Ref. [68], but on a different vertical scale. Notice that the scales on the vertical axes are, in general, different for each partial wave as well.

In Fig. 5 we display the correlation function for each uncoupled N-N partial wave, defined by

$$f_{\rm corr}(r) \equiv \frac{\widetilde{u}^{SJ}_{k,l}(r)}{\hat{j}_l(kr)}. \tag{38}$$

Again, the most remarkable feature of these plots is the little dependence of the correlation function on the different CM momenta of the nucleon pair. The boldest dependence on the CM momenta, especially close to the origin ($r = 0$), occurs

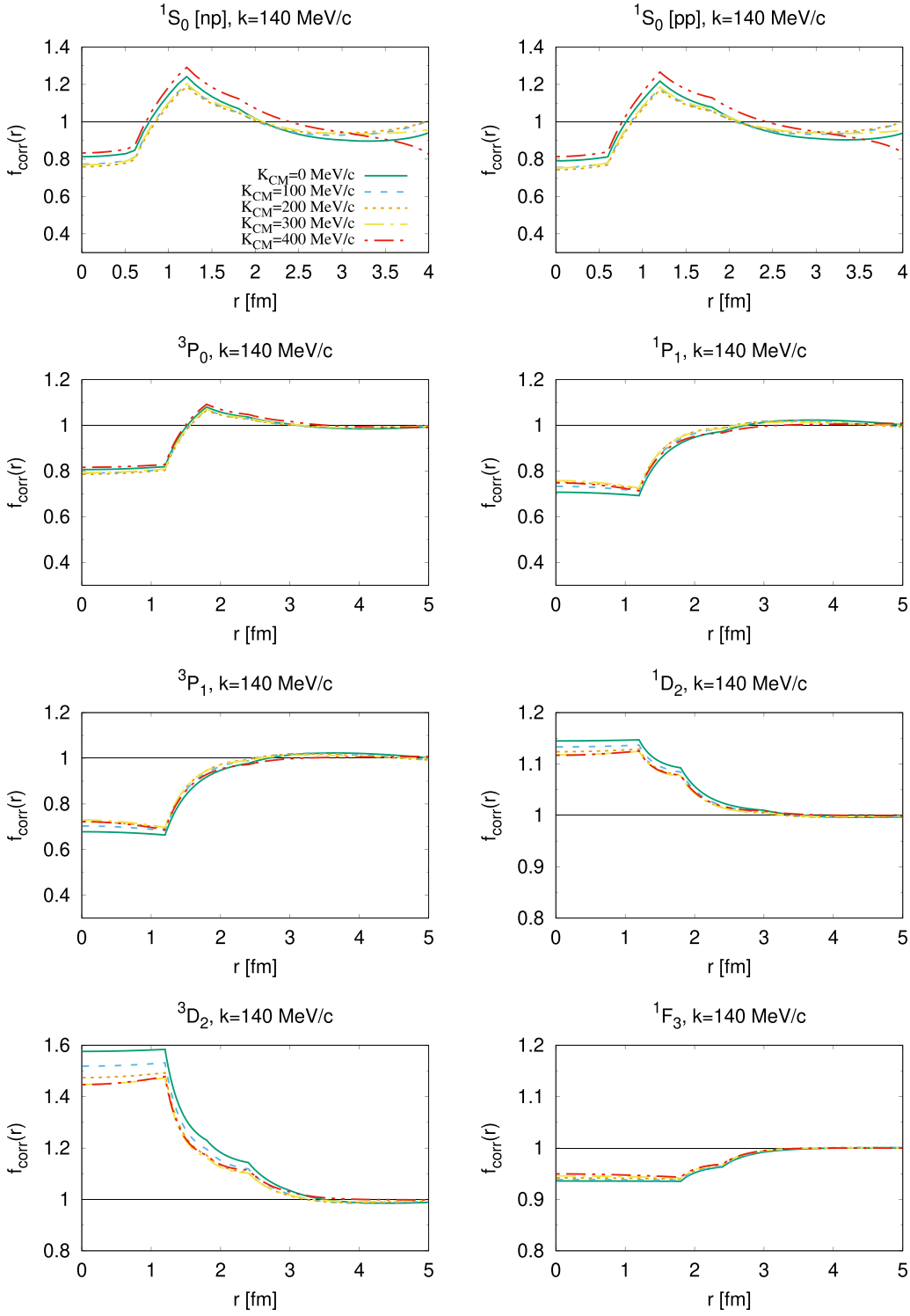

FIG. 5. Correlation functions $f_{\rm corr}(r) \equiv \frac{\widetilde{u}^{SJ}_{k,l}(r)}{\hat{j}_l(kr)}$ for the uncoupled N-N partial waves, $l' = l$. The results are given for relative momentum $k = 140$ MeV/c and for the same values of the CM momentum as in Figs. 3 and 4. The results for $K_{\rm CM} = 0$ MeV/c (solid green lines) are the same as those shown in Fig. 2 of Ref. [68].

for the $^3D_2$ partial wave. The departures of the correlation functions from unity occur only at short distances, and these functions rapidly approach 1 at larger distances, which means that the perturbed solutions reach the free ones without any phase-shift:

$$f_{\rm corr}(r) \longrightarrow 1 \iff \widetilde{u}^{SJ}_{k,l}(r) \longrightarrow \hat{j}_l(kr) \quad \text{for } r > 3 \text{ fm}. \tag{39}$$

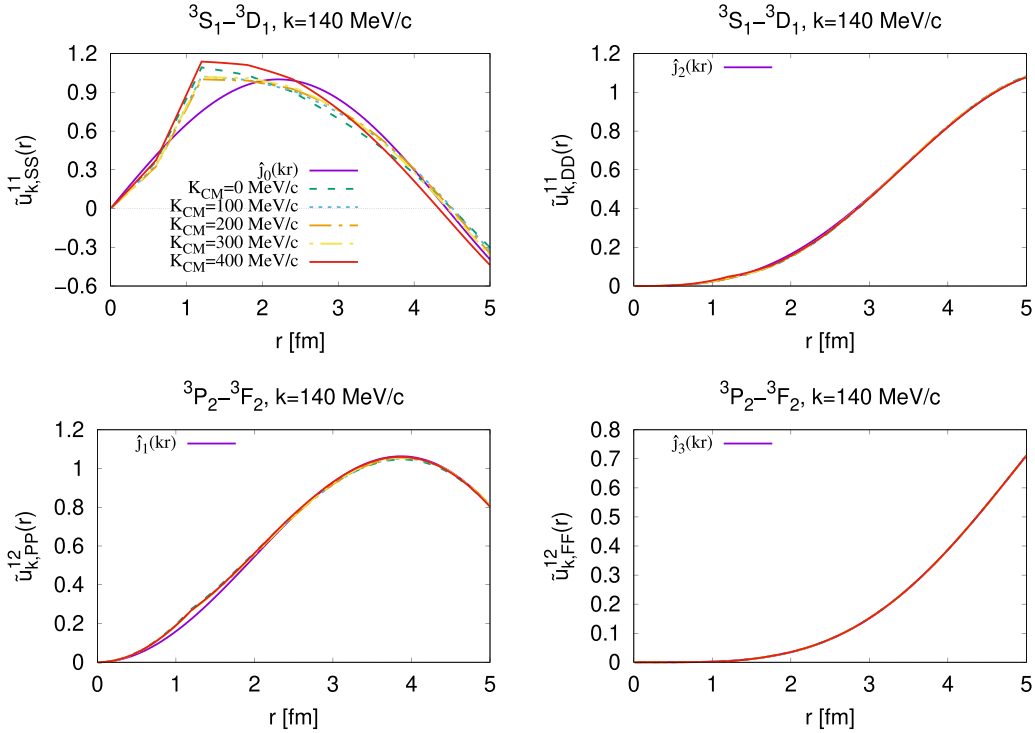

FIG. 6. Perturbed radial diagonal wave functions $\widetilde{u}^{SJ}_{k,l\,l}(r)$ (for $l' = l$) for the coupled N-N partial waves $^3S_1$ - $^3D_1$ and $^3P_2$ - $^3F_2$. The results are given for relative momentum $k = 140$ MeV/c, and for each partial wave the free solutions $\hat{j}_l(kr)$ to which they trend when $r \to \infty$ are shown, as well as those for different values of the CM momentum. Although not distinguishable in all the panels, the curves labeled in the key of the upper left panel are also displayed in all the others.

Indeed, special attention must be paid to the zeros of the reduced spherical Bessel functions $\hat{j}_l(kr)$ in the analysis. At these zeros, the perturbed wave functions can have numerical uncertainties that may give the impression of a nonzero phase shift at long distances, even although the correlation functions approach unity. This is due to two reasons: numerical uncertainties in the calculation of $\widetilde{u}^{SJ}_{k,l}(r)$ at the nodes, that prevent an exact cancellation of both nodes when numerically evaluating Eq. (38), and the fact that the perturbed wave function truly converges on the free one precisely at *very long distances*, thus the quotient at the nodes is never exactly 1. This is, for example, the reason for plotting the correlation function for the $^1S_0$ partial wave of Fig. 5 only up to 4 fm, precisely because the node for the value of k considered in the same panels of Fig. 3 appears between 4 and 5 fm.

In Fig. 6 we show the diagonal $l = l'$ radial wave functions for the coupled N-N partial waves $^3S_1$ - $^3D_1$ and $^3P_2$ - $^3F_2$, for different values of the CM momentum of the two-nucleon system and for a relative momentum of $k = 140$ MeV/c. For the coupled channels, the notation SS refers to the partial wave with $l = l' = 0$, SD refers to the partial wave with $l = 0$ and $l' = 2$, and so on, following the usual spectroscopic notation for the orbital angular momenta. The general trend with respect to the dependence of them on the CM momentum is similar to that of the uncoupled partial waves, i.e., there is little dependence on the value of the CM momentum. And, the departure from the free solution is more remarkable for the lower values of the orbital angular momenta l. The most striking dependence on the CM momentum occurs for the SS wave at the cusp, but it is also similar to the case of the uncoupled $^1S_0$ partial wave (cf. first panels of Figs. 3 and 6).

In Fig. 7 we show the defect diagonal ($l = l'$) radial wave functions for the N-N coupled channels, together with their coupled off-diagonal ($l \neq l'$) partners on the right panels. The most remarkable feature is that the size of the distortion due to the short-range correlations is similar in the partial waves which are coupled between themselves, i.e., those corresponding to the left and right panels in each row of the figure. Furthermore, the distortions are more sizable for the lower l partial waves, as already remarked in the discussion of Fig. 6; and, in general, there is little dependence on the CM momentum of the nucleon pair, although this can seem enhanced because of the scales shown in Fig. 7 with respect to those of Fig. 6.

In Fig. 8 we show the correlation functions for the diagonal ($l = l'$) coupled N-N partial waves. Their behavior is, in general, similar to that of the uncoupled partial waves, i.e., their departure from 1 at short distances is very similar in magnitude, and there is little dependence on the CM momentum of the nucleon pair, except for the DD radial wave function of the $^3S_1$ - $^3D_1$ coupled channel, where there is a more pronounced dependence on the CM momentum for the highest one shown in the upper right panel of Fig. 8. Nonetheless, similar behaviors can be also observed in the $^3D_2$ channel of Fig. 5 or even, to a lesser extent, in the PP component of the $^3P_2$ - $^3F_2$ channel, shown in the bottom left panel of Fig. 8.

In Fig. 9 we observe the long-range behavior of the defect coupled radial wave functions for $K_{CM} = 0$. The left panels

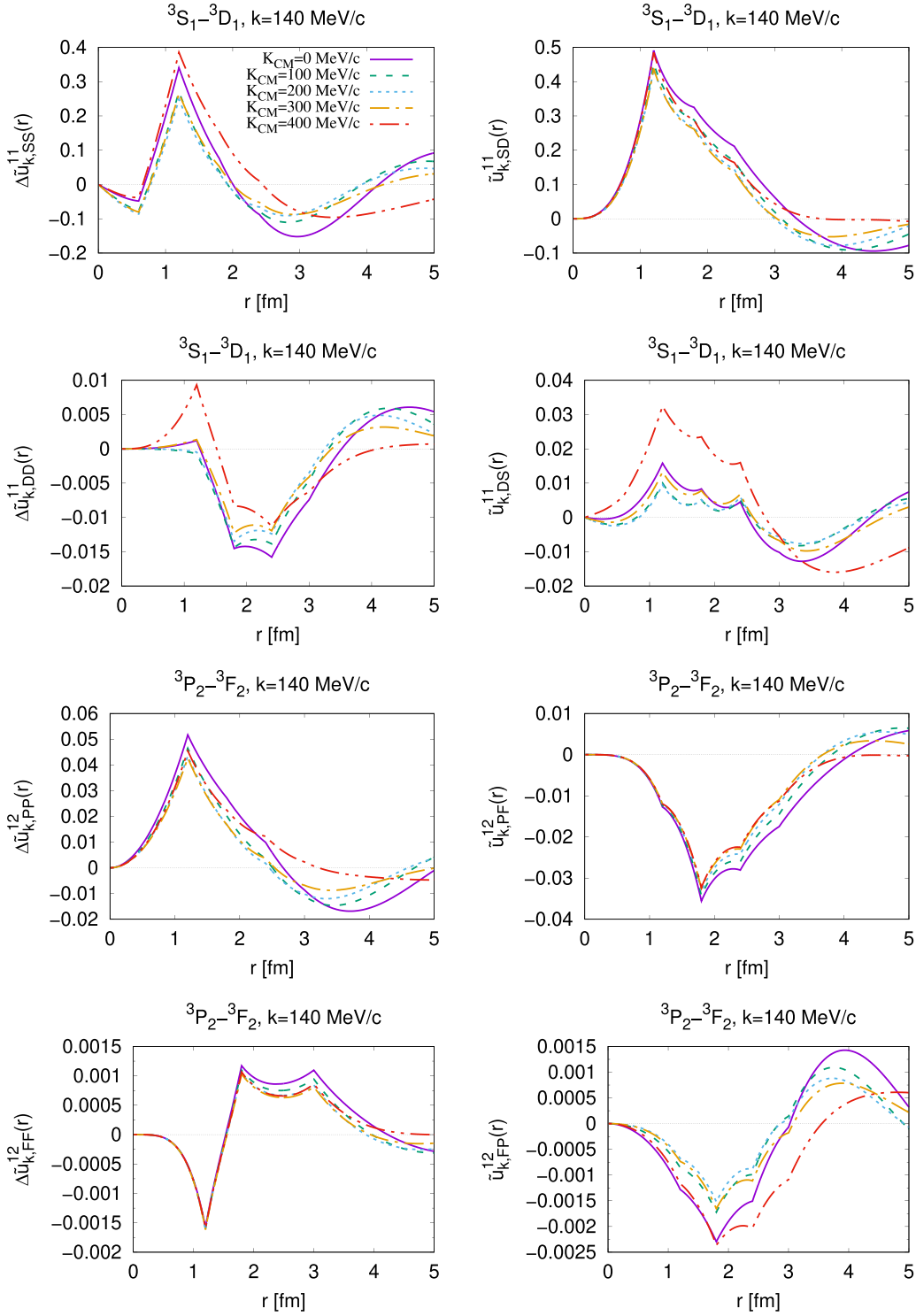

FIG. 7. Defect diagonal ($l = l'$) wave functions $\Delta\tilde{u}^{SJ}_{k,ll}(r) \equiv \tilde{u}^{SJ}_{k,ll}(r) - \hat{j}_l(kr)$ (left panels) and off-diagonal wave functions $\tilde{u}^{SJ}_{k,ll'}(r)$ (for $l \neq l'$) (right panels) for the coupled N-N partial waves $^3S_1$ - $^3D_1$ and $^3P_2$ - $^3F_2$. The results are given for relative momentum $k = 140$ MeV/c and for the same values of the CM momentum as in Fig. 6.

compare the $(J-1, J-1)$ waves to the $(J-1, J+1)$ ones, while in the right panels the $(J+1, J+1)$ waves are compared to the $(J+1, J-1)$ ones. In each panel, both functions approach zero in an oscillatory manner, as expected. However, this decrease occurs very slowly in the scale of each plot, indicating a gradual decrease in amplitude as the distance increases. It is worth noticing that the coupled waves shown in each panel have the same order of magnitude, in concordance with the findings discussed in Fig. 7. This order of magnitude, which is a measure of their deviation with respect to

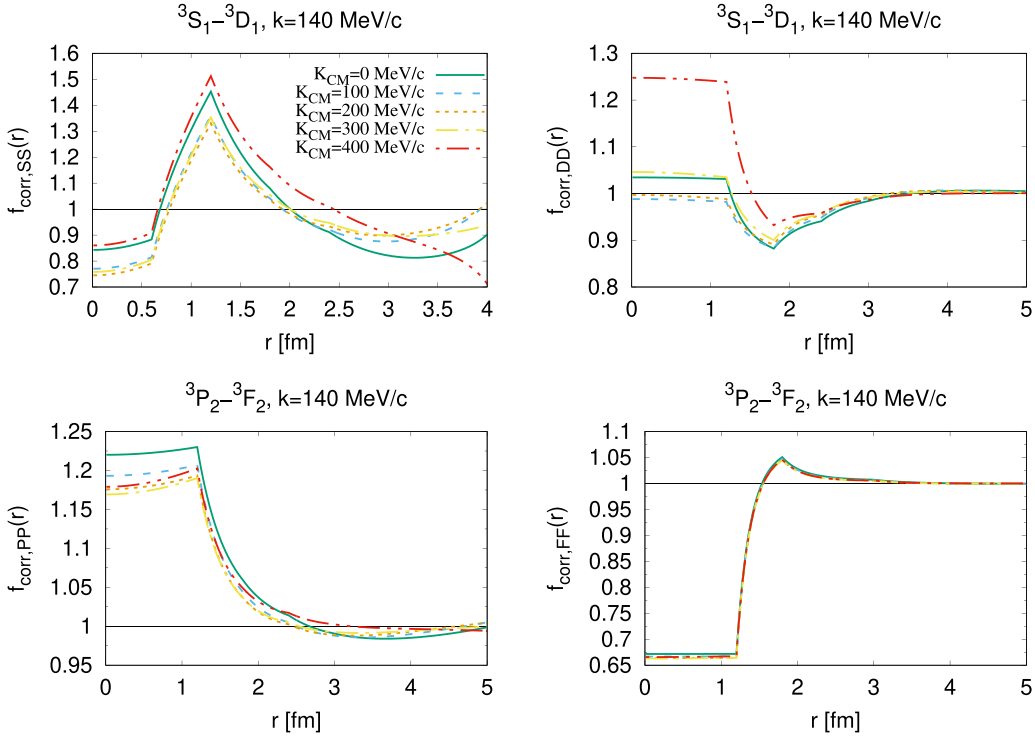

FIG. 8. Correlation functions $f_{\rm corr}(r)$ for the diagonal ($l = l'$) wave functions, whose trend when $r \to \infty$ should be 1, for the coupled N-N partial waves $^3S_1$ - $^3D_1$ and $^3P_2$ - $^3F_2$. The results are given for relative momentum $k = 140$ MeV/c and for the same values of the CM momentum as in Figs. 6 and 7.

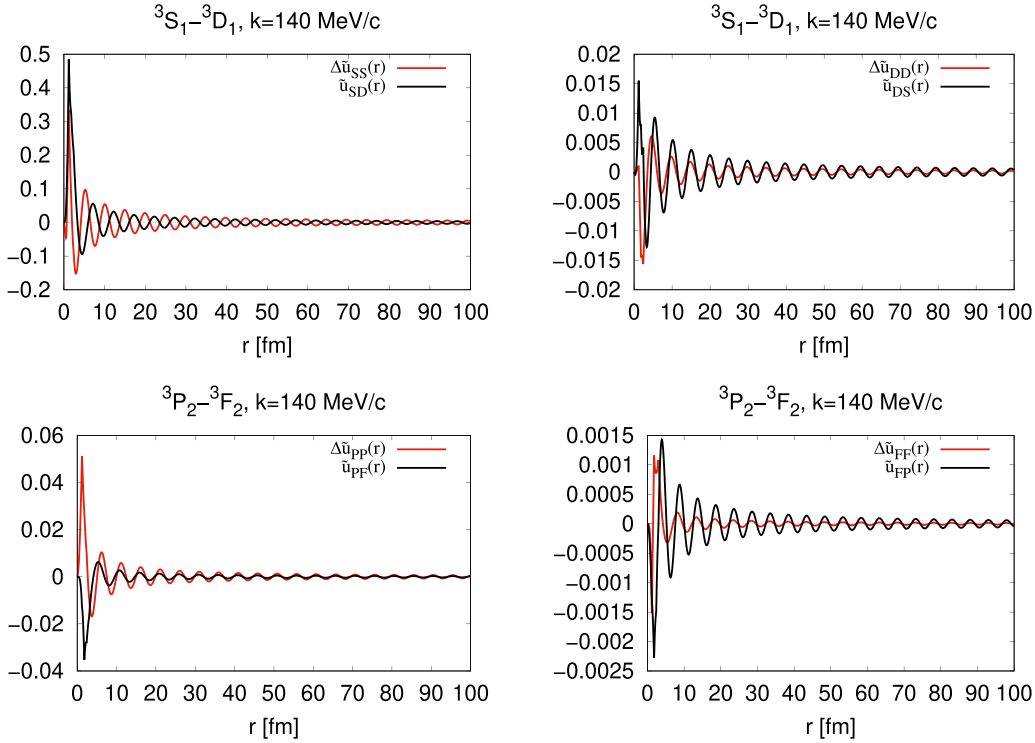

FIG. 9. Long range ($r \to \infty$) behavior of the defect diagonal wave functions and the off-diagonal ones for the N-N coupled channels, and for $K_{\rm CM} = 0$. All of them go to zero, but are slowly converging on the scale of each figure. This means that there is no phase shift in the B-G wave functions $\tilde{u}_{ll}(r)$ with respect to the free solution when $r \to \infty$.

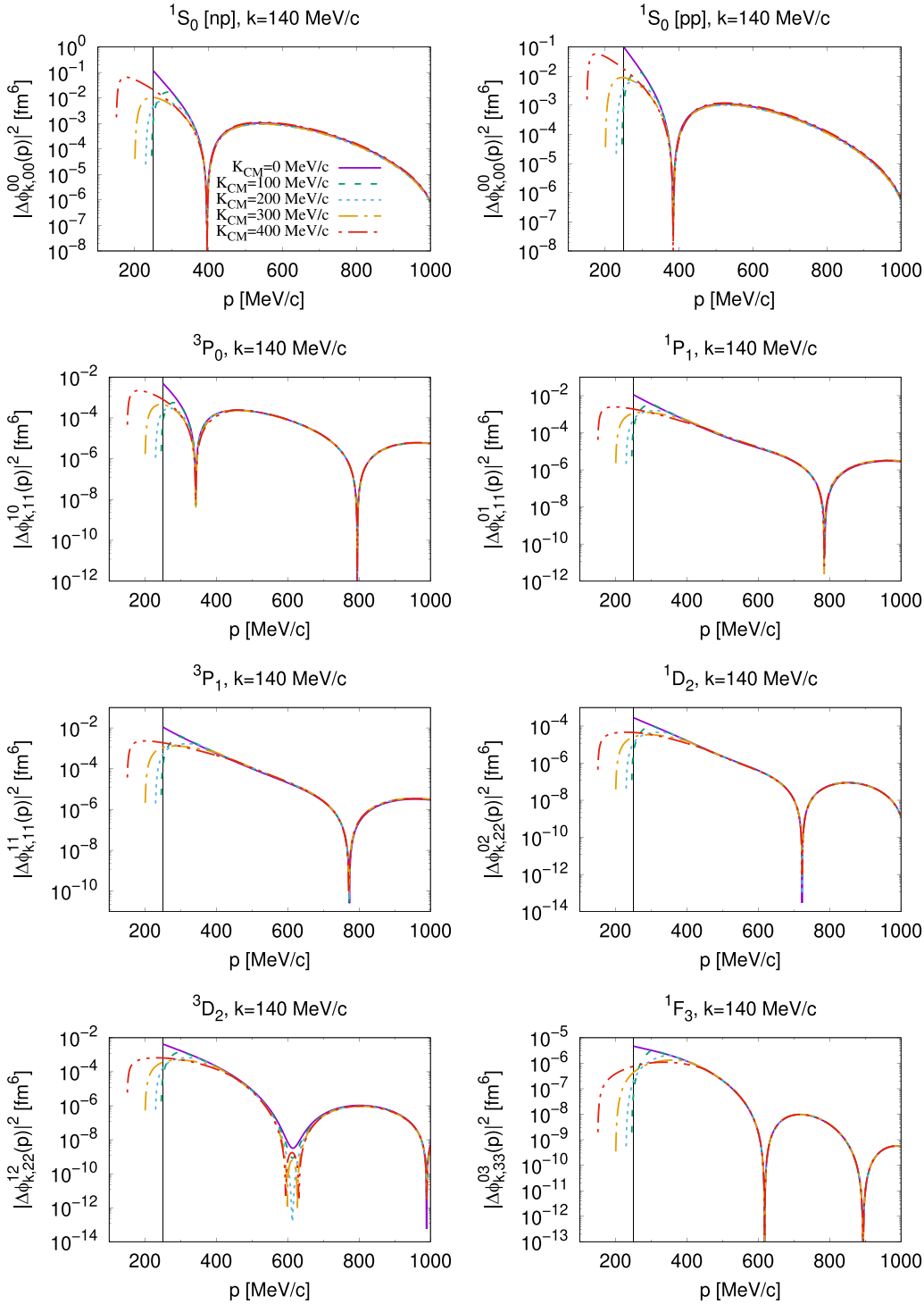

FIG. 10. "Radial" wave functions $|\Delta\phi^{SJ}_{k,l'l}(p)|^2$ for the uncoupled N-N partial waves, i.e., for $l = l'$. The results are given for relative momentum $k = 140$ MeV/c, and for different values of the CM momentum as labeled in the key of the first panel. The results for $K_{\rm CM} = 0$ MeV/c (solid purple lines) are the same as those shown in the upper panel of Fig. 6 of Ref. [68].

their free asymptotic behavior, and therefore a measure of the importance of the short-range correlations in each channel, is higher the lower the orbital angular momentum l is, in perfect accordance with the findings of the discussion of Fig. 7 as well.

B. "Radial" wave functions in momentum representation: High-momentum components

In Figures 10 and 11 we show the square of the high-momentum component of the "radial" wave function $|\Delta\phi^{SJ}_{k,l'l}(p)|^2$ in momentum space [see Eq. (28)], for different

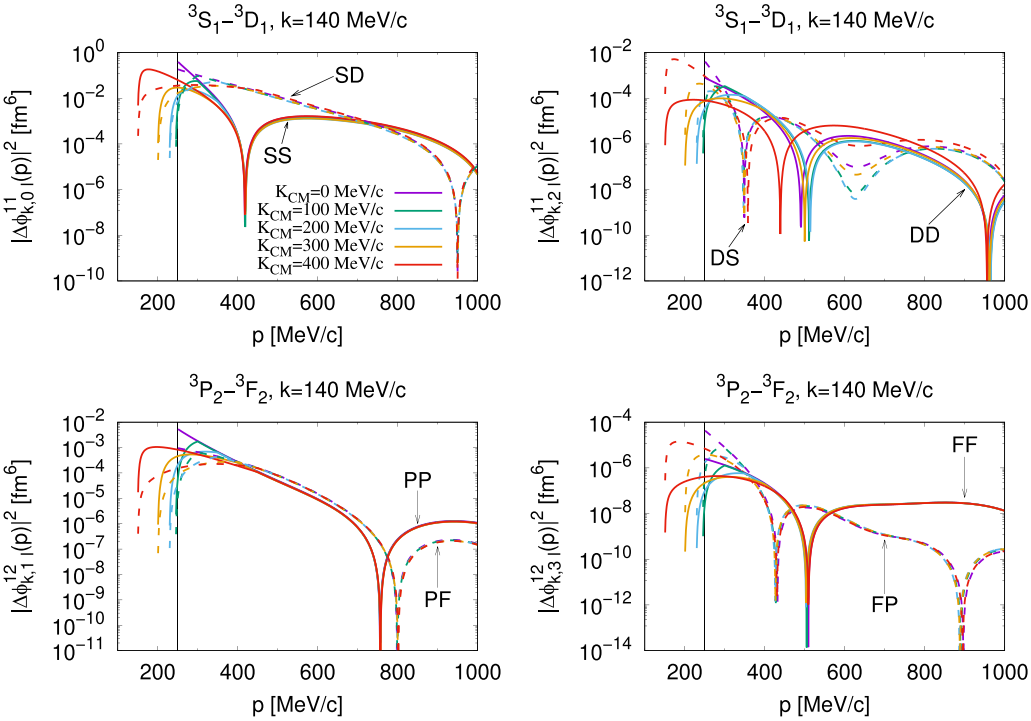

FIG. 11. "Radial" wave functions $|\Delta\phi^{SJ}_{k,l'l}(p)|^2$ for the coupled N-N partial waves. The results are given for relative momentum $k = 140$ MeV/c, and for different values of the CM momentum as labeled in different colors in the key of the first panel. The solid lines correspond to the diagonal $l' = l$ waves, while the dashed lines are the results corresponding to the off-diagonal ($l' \neq l$) coupled waves.

CM momenta of the nucleon pair, of the uncoupled and coupled N-N partial waves, respectively. The vertical black lines in the different panels at $p = 250$ MeV/c mark the position of the Fermi momentum. These show the high-momentum components in the relative wave function due to the short-range correlations.

As already discussed in Fig. 2, the angle-averaged Pauli-blocking function appearing in Eq. (28) is always a piecewise function bounded between 0 and 1, depending on the values of the CM momentum $K_{\rm CM}$ and the probed relative one p of the nucleon pair. Therefore, if one wants to look at the effects produced in the high-momentum components by the influence of the CM momentum on the radial wave functions at the grid points, one should look at regions of p in Figs. 10 and 11 where the angle-averaged Pauli blocking operator does not depend at all on $K_{\rm CM}$. These regions of p where $\overline{Q}(K_{\rm CM}, p) = 1$ correspond to zone (c) in Fig. 1, i.e., when $p > k_F + \frac{K_{\rm CM}}{2}$. In the most unfavorable situation, we should look at $p > 2k_F = 500$ MeV/c in Figs. 10 and 11.

In this region of values of p, the only observable differences between the curves for distinct CM momenta can only come from the differences in the radial wave functions at the grid points r_i, shown in Figs. 3, 6, and the right panels of Fig. 7. However, if we look in Figs. 10 and 11 at $p \gtrsim 500$ MeV/c, we do not observe almost any difference between the curves for distinct CM momenta, except for the particular cases of the $^3D_2$ and the $DS - DD$ coupled components of the $^3S_1$ - $^3D_1$ partial waves, which will be explained later. Therefore, the conclusion is that the differences due to the CM momentum dependence on the radial wave functions (even the largest ones for the low l partial waves) observed in Figs. 3, 4, 6, and 7 mostly completely irrelevant for the tail of high-momentum components ($p \gtrsim 2k_F$) in the relative wave function of the nucleon pair. This points out the universality of SRCs or, *at least, that the global motion state of the nucleon pair has negligible influence in the tail of high momentum components.*

However, if we observe Figs. 10 and 11 for $p \lesssim 2k_F = 500$ MeV/c, the angle-averaged Pauli-blocking function, $\overline{Q}(K_{\rm CM}, p)$ of Eq. (28), starts to play a significant role. For a fixed value of the CM momentum of the pair, when diminishing the probed relative momentum p, we are entering into region (b) of Fig. 1 from region (c) of the same figure. And, in region (b) of Fig. 1, the value of the $\overline{Q}(K_{\rm CM}, p)$ function starts to get reduced from 1 at the right line $p = k_F + \frac{K_{\rm CM}}{2}$ to 0 at the ellipse $p = \sqrt{k_F^2 - \frac{K_{\rm CM}^2}{4}}$.

This reduction in the value of the angle-averaged Pauli-blocking function gets reflected in the departures from the purple lines of almost all the curves for $K_{\rm CM} > 0$ MeV/c in Figs. 10 and 11 at different values of p. The smaller the value of $K_{\rm CM}$ is, the smaller the value of p is at the point where the deviation from the purple curves occurs. This fact can be easily understood looking again at Fig. 1. Indeed, if we plot imaginary vertical lines in Fig. 1 at the CM momenta depicted in Figs. 10 and 11, we observe that region (b) along these imaginary vertical lines starts to become larger when the CM momentum increases. This is so because the right line is growing and the ellipse is diminishing. This causes the point of deviation from the purple curves (corresponding to

$K_{\rm CM} = 0$) in Figs. 10 and 11 to be larger in the p variable when the CM momentum is also larger. In fact, the exact point of deviation from the purple curves occurs at $p_{\rm dev}(K_{\rm CM}) = k_F + \frac{K_{\rm CM}}{2}$, which of course depends on the value of the CM momentum.

Another interesting features that can be observed in Figs. 10 and 11 is that for $K_{\rm CM} > 0$ MeV/c the high-momentum distributions intrude below the Fermi momentum marked by the vertical lines on the same figures. This, again, can be easily understood by looking at Fig. 1: for $K_{\rm CM} > 0$ MeV/c, the points p below which the high-momentum distributions are zero correspond to the ellipse points, and these are always below the Fermi momentum when $K_{\rm CM} > 0$. The particular case when $K_{\rm CM} = 0$ corresponds to the purple curves in Figs. 10 and 11, and for this CM momentum the high-momentum distribution is zero exactly at $p = k_F$. However, there are never high-momentum distributions for $p < k$. The only low momentum component is the unperturbed component for $p = k$, represented by the Dirac delta function in Eq. (27).

Another interesting point is that the high-momentum distributions $|\Delta\phi^{SJ}_{k,l'l}(p)|^2$ are continuous at the deviation points from the purple lines, $p_{\rm dev}(K_{\rm CM})$, but their derivatives with respect to p at these points are not continuous. This fact is completely related to the discontinuity in the derivative of the angle-averaged Pauli-blocking function (see Fig. 2) at the joining point between regions (b) and (c) of Fig. 1 along a vertical line for a constant value of $K_{\rm CM}$. This feature was already discussed in point 5 at the end of Sec. II B. In particular, this effect is very clearly observable for the curves of Figs. 10 and 11 corresponding to $K_{\rm CM} = 100$ MeV/c, whose angle-averaged Pauli-blocking function has a behavior very similar to that of the second panel ($K_{\rm CM} = 0.5\,k_F$) in Fig. 2. Indeed, in these cases of low CM momenta, the discontinuities in the derivative of the $\overline{Q}(K_{\rm CM}, p)$ function at $p_{\rm dev} = k_F + \frac{K_{\rm CM}}{2}$ are much more pronounced than for larger CM momenta, as can be observed in the different panels of Fig. 2 (notice that for the first panels the slope of the transition curve between 0 and 1 is much steeper than for the last panels).

The case of the $^3D_2$ partial wave high-momentum distribution shown in Fig. 10 deserves a separate explanation for its behavior at $p \approx 600$ MeV/c. This is the region of p values where the angle-averaged Pauli-blocking function is equal to 1, and therefore any difference between the curves for distinct CM momenta can be solely ascribed to differences in the perturbed radial wave functions at the grid points $[\widetilde{u}^{12}_{k,2}(r_i)]$ for the different CM momenta of the nucleon pair, as appear in Eq. (28). The explanation is as follows: when $K_{\rm CM} = 0$ MeV/c, the corresponding curve (purple line) in Fig. 10 does not have a node at $p \approx 600$ MeV/c, but a local minimum very close to 0; however, the differences in the perturbed radial wave functions at the grid points when varying the CM momentum make this local minimum become also a node for $K_{\rm CM} \approx 200$ MeV/c (short-dashed blue line). Finally, if one increases the value of the CM momentum above 200 MeV/c, the minimum of the function $\Delta\phi^{12}_{k,22}(p)$ at $p \approx 600$ MeV/c starts to have negative values and cuts the p axis at two nodes very close to $p \approx 600$ MeV/c, but each one of them at one side of the negative minimum. This gives the particular pattern shown in the $^3D_2$ panel of Fig. 10 for the square of the function $\Delta\phi^{12}_{k,22}(p)$ around $p \approx 600$ MeV/c, presenting two very close nodes for $K_{\rm CM} = 300$ and 400 MeV/c.

The differences observed in the $DS - DD$ coupled waves of the $^3S_1$ - $^3D_1$ (top right panel of Fig. 11) channel, particularly between the case of $K_{\rm CM} = 400$ MeV/c and the other CM momenta, can be explained by looking at the defect radial wave functions for that channel in Fig. 7 (second line plots of that figure). In this case, in contrast to the others of the same figure, one can observe a relevant difference at short distances between the curve for $K_{\rm CM} = 400$ MeV/c and those for the other CM momenta. This is particularly evident for the DS relative wave function. Notice that, despite being basically D waves, the magnitude of the distortion at short distances is quite similar to that of the $PP - PF$ ($l = 1$) coupled waves. However, for this latter case, all the distortions depend little on the CM momentum, while in the $DS - DD$ case there is a significant difference between the case with $K_{\rm CM} = 400$ MeV/c and the other CM momenta configurations, whose curves show a softer dependence on the total momentum. This makes the high-momentum components for this DS-DD coupled channel depend substantially more on the CM momentum, especially for the DS component at $p \simeq 625$ MeV/c (note that the vertical scales in Fig. 11 are logarithmic).

In Fig. 12 we display the total high-momentum distributions of a nucleon pair with initial relative momentum k and spin S, for $p > k$, which we define as:

$$\bar{\rho}^S_k(p) = 4\pi\,(2S+1)\rho^S_{k,K_{\rm CM}}(p) = \sum_{l,l',J} \Delta(JSl')\,(2J+1)\left|\Delta\phi^{SJ}_{k,l'l}(p)\right|^2, \qquad (40)$$

where $\rho^S_{k,K_{\rm CM}}(p)$ is given by Eq. (35) but replacing $\phi^{SJ}_{k,l'l}$ by $\Delta\phi^{SJ}_{k,l'l}$. We show results for np (solid lines) and pp pairs (dashed lines) at relative momentum of $k = 140$ MeV/c for different CM momenta of the pair, as labeled in the key of the top left panel of Fig. 12. The purpose of giving the quantity $\bar{\rho}^S_k(p)$ is because it is directly comparable with Eq. (43) of Ref. [68] and with Figs. 8 and 9 (upper panel) of the same reference.

The upper left panel of Fig. 12 shows the total high-momentum density distribution (summed over the different partial waves) for correlated np and pp pairs with total spin $S = 0$. Both np and pp momentum distributions are very similar in the intermediate region of probed relative momentum $450 \lesssim p \lesssim 850$ MeV/c. This is due to the fact that the $^1P_1$ contribution, which is present in np pairs with $S = 0$ but not in pp pairs with the same total spin, is quite irrelevant in this region of p if compared with the dominant component coming from the $^1S_0$ partial wave. However, the differences between np and pp pairs are patent at $p \approx 400$ MeV/c, where the dominant $^1S_0$ partial wave has a node, and then the $^1P_1$ contribution makes the difference between np and pp pairs, because for the latter only the $^1D_2$ partial wave can be added (due to antisymmetry considerations of the relative wave function for two identical fermions), and its contribution is far less important than that of the $^1P_1$ channel.

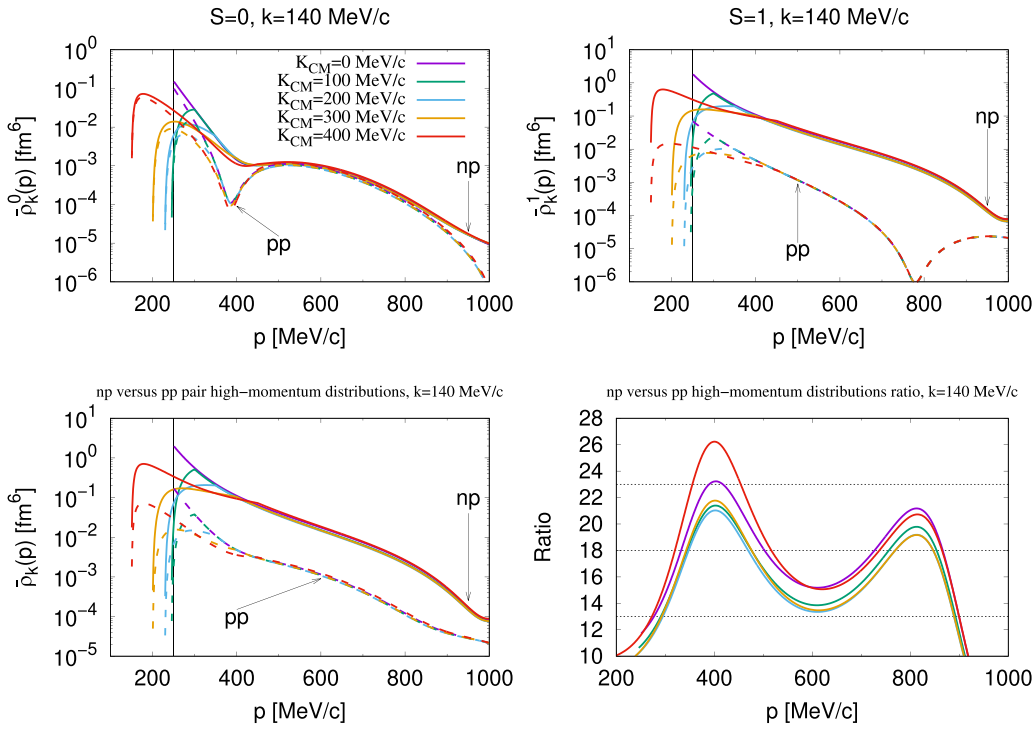

FIG. 12. Probability densities of high-momentum components per nucleon pair $\bar{\rho}_k^S(p)$ [see definition given in Eq. (40)] for $S = 0$ (upper left panel), $S = 1$ (upper right panel), and summing the contributions from the two spin configurations (lower left panel). The results are given for relative momentum $k = 140$ MeV/c, and for different values of the CM momentum as labeled in the key of the first panel. The solid lines refer to momentum distributions of np pairs, while the dashed lines correspond to pp pairs. The results for $K_{\rm CM} = 0$ MeV/c (purple lines) are essentially the same as those shown in Fig. 8 and in the upper panel of Fig. 9 of Ref. [68]. Therefore, these curves are directly comparable with the quantity defined in Eq. (43) of Ref. [68]. On the other hand, the lower right panel corresponds to the ratio of high-momentum density distribution of np over pp pairs, for the same CM momenta displayed in the other panels. This is straightforwardly comparable with the lower panel of Fig. 9 in Ref. [68]. The ratios are, generally, 18 ± 5 for a wide range of high momentum components and are almost insensitive to the CM momenta of the nucleon pair.

In the upper right panel of Fig. 12 we show the same total high-momentum distributions for correlated np and pp pairs in the triplet spin state, $S = 1$. In this case the differences between np and pp pairs are much clearer in the whole range of p. This is because for pp pairs in the triplet state only odd l partial waves contribute (P and F waves), while for np pairs all triplet partial waves are summed, especially the most relevant ones, such as the $^3S_1$ - $^3D_1$ coupled channel. Basically, the presence of the $^3S_1$ - $^3D_1$ channel in the np high-momentum distribution, while not in the pp one, makes the former much larger, in general by several orders of magnitude.

In the lower left panel of Fig. 12, we can observe the sum of both singlet and triplet contributions for the high-momentum distributions of np and pp pairs. This panel represents the high-momentum density distribution of a nucleon pair regardless of its total spin state. It is evident that the np distribution is approximately an order of magnitude larger than the pp distribution. This observation is consistent with the findings of Ref. [68], which also reported a similar trend in its Figs. 9 and 10.

It is also worth pointing out that the so-far-discussed three panels shown in Fig. 12 share several common features with those of Figs. 10 and 11, namely, very little dependence of the high-momentum distributions on the CM momentum of the pair for $p \gtrsim k_F + \frac{K_{\rm CM}}{2}$; intrusion of the momentum distributions below the Fermi momentum for $K_{\rm CM} > 0$; and, finally, it is very clear that the pair momentum distributions are continuous at the deviation points $p_{\rm dev}(K_{\rm CM}) = k_F + \frac{K_{\rm CM}}{2}$, but not their derivatives at these points. This latter fact has been already discussed in relation with Fig. 2.

Finally, in the lower right panel of Fig. 12 we show the ratio $\frac{\bar{\rho}_k^{\rm np}(p)}{\bar{\rho}_k^{\rm pp}(p)}$ for a relative momentum of the pair of $k = 140$ MeV/c and for the five different CM momenta displayed in the other panels of the same figure, as a function of the probed high momentum p. Again, the ratio is quite insensitive to the CM momenta of the nucleon pair, and, for a wide range of probed high momentum p, the ratio is 18 ± 5, which is the claimed averaged ratio measured in Ref. [21] for the ground state of the ^{12}C nucleus.

To finish, in Fig. 13 we present a comparative analysis of our results with those obtained from a realistic calculation in a finite nucleus using the variational Monte Carlo (VMC) approach, as reported in Ref. [50]. The comparison is focused on the relative-momentum densities for neutron-proton (np) and proton-proton (pp) pairs, which were determined from the solution of the Bethe-Goldstone equation for a center-of-mass momentum $K_{\rm CM}$ of 0 and an initial relative momentum k of 140 MeV/c. To provide a comprehensive assessment, we compared our findings with the high momentum pair

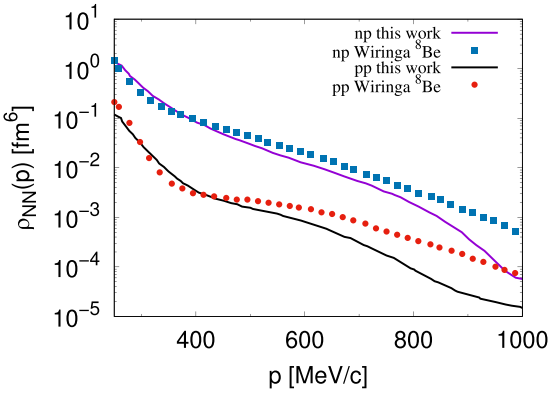

FIG. 13. Comparison of the np and pp pairs' high-momentum distributions of this work, for $K_{\rm CM} = 0$ and $k = 140$ MeV/c, with those for ^{8}Be nucleus found in Fig. 15 of Ref. [50], calculated within the variational Monte Carlo (VMC) approach. The two-nucleon momentum densities are plotted as functions of the high relative momentum p. The high momentum np distributions have been normalized to 1 fm^3.

distribution of the nucleus ^{8}Be, specifically for $K_{\rm CM} = 0$, as depicted in Fig. 15 of Ref. [50].

It is important to note that the pair momentum distribution presented in Ref. [50] involves the utilization of the full nuclear wave function. Establishing a direct and straightforward relationship between this distribution and the solution of the Bethe-Goldstone equation for a specific pair with an initial relative momentum k is not a trivial task, and deserves further investigation.

Here we make some remarks to explain how this comparison was carried out. As our two-nucleon densities have, in general, a weak dependence (see Fig. 10 of Ref. [68]) on the initial relative momentum k of the pair, we have chosen again $k = 140$ MeV/c to perform the comparison, which is an intermediate value for the initial relative momentum of the pair when its total momentum is zero. In the comparison with the nucleon-pair momentum distributions in ^{8}Be for back-to-back ($K_{\rm CM} = 0$) pairs found in Fig. 15 of Ref. [50], we have disregarded the part of the distributions below $q < k_F = \frac{250}{197.33} = 1.267$ fm^{-1}, for normalization purposes, in order to focus on the high momentum contribution.

However, given that our pair momentum distributions exhibit only weak dependence on the precise value of k, and under the reasonable assumption that the contribution from high momenta primarily reflects short-distance behavior which is relatively independent on the nuclear size, the trends provided by Fig. 13 offer a valuable insight into the comparison between np and pp pair distributions and what is expected in finite nuclei. Indeed, we observe that the relationship between the np and pp distributions in our study approximates the same trend observed in Ref. [50].

What we have done is to normalize our np-pair distribution, for $K_{\rm CM} = 0$, taken from the lower left panel of Fig. 12, in such a way that the integral $\int \bar{\rho}_{\rm np}(p)\, p^2\, dp = 1$ fm^3. And we have done exactly the same for the np-pair distribution of Fig. 15 of Ref. [50] starting from $q \simeq 1.267$ fm^{-1}. Later, we scaled the pp-pair momentum distributions in both models accordingly with the normalization factors found in the previous procedure, in order to keep the proportionality between the nucleon-pair momentum densities. Although in Fig. 15 of Ref. [50] there are no units on the y axis for the momentum distribution, according to Eq. (6) of the same reference the right units for the nucleon-pair distribution of that figure are fm^6 [145].

The result of the comparison can be observed in Fig. 13, where our results are shown as solid lines, while the results of Ref. [50] are displayed as filled squares for the np-pair distribution, and as filled circles for the pp one. For relative intermediate momentum, $p \leqslant 500$ MeV/c, the respective momentum distributions look quite similar in size and shape. However, for larger relative momenta, they start to differ significantly: the nucleon-pair momentum distributions calculated in ^{8}Be start to be larger by almost one order of magnitude with respect to those of this work for nuclear matter. However, recent calculations [146,147] with the same methods based on chiral interactions clearly show a trend in qualitative agreement similar to that presented in Fig. 13. Presumably, this feature is related to the comparatively harder core of the AV18 potential, as compared to the current chiral interactions and our coarse-grained potential.

Finally, this approximation suggests that, despite the inherent complexities associated with a full nuclear wave function, and differences in nuclear matter and finite nuclei, our theoretical framework captures important aspects of neutron-proton and proton-proton pair interactions. These results are in themselves remarkable and suggest a quantitative connection between nuclear matter and finite nuclei.

V. CONCLUSIONS

In this work we have extended our previous studies [63,68] about the effects of SRCs on the high-momentum components of the relative wave function for a nucleon pair in nuclear matter. The extension amounts to taking the angular average of the Pauli-blocking operator for the case with $K_{\rm CM} \neq 0$, and observing its effects on the tail of relative high-momentum components.

Our findings indicate minimal dependence on the CM momentum of the nucleon pair in the majority of plots presented in this paper. This consistency is observed in various aspects, including the relative wave function at short distances, correlation functions in the proximity of the origin, and defect wave functions. Furthermore, we also observe limited sensitivity to the overall CM momentum of the pair when examining the higher-momentum components of the relative wave function. This holds true as long as the probed relative momentum p exceeds $2k_F$, where k_F represents the Fermi momentum. This last finding is consistent with the universality of SRCs and with the factorization *Ansätze* used in the literature to express the pair momentum distribution as a product of the momentum distribution of the CM times the momentum distribution of the relative motion, the last being a universal function [29,57,58,67,148].

In our case, the momentum distribution of the CM motion can be described by a three-dimensional Dirac delta function. This is due to the conservation of total momentum in the

Bethe-Goldstone equation. In finite nuclei, the momentum distribution of the CM is broadened. This broadening has been observed and modeled using a three-dimensional Gaussian function in Ref. [29]. This approach is reasonable as the Dirac delta function can be considered as a limiting case of a Gaussian function with an infinitesimally small width.

Therefore, it is reasonable to assume that our findings regarding the independence of the relative high-momentum distribution of a pair on the CM momentum could be extrapolated to finite nuclei. This assumption holds true as long as the distribution is generated by universal short-range correlations, considering the inherent limitations in obtaining an exact resolution of the problem in such systems.

ACKNOWLEDGMENTS

This work was partially supported by Grant No. PID2020-114767GB-I00 funded by MCIN/AEI/10.13039/501100011033, by FEDER/Junta de Andalucía-Consejería de Transformación Económica, Industria, Conocimiento y Universidades/A-FQM-390-UGR20, and by Junta de Andalucía (Grant No. FQM-225). The authors of this work are deeply indebted to Prof. Robert B. Wiringa for many clarifications about the interpretation of his results, especially in connection with the discussion of the last figure of the present paper.

APPENDIX A: FORMAL DERIVATION OF B-G EQUATION FOR TOTAL AND RELATIVE PERTURBED STATES

In this Appendix we give the formal derivation of Eqs. (5) and (7) starting from Eq. (1). If we apply Eq. (1) in operator form to a ket in the CM and relative momenta representation $|\mathbf{K}_{\rm CM}, \mathbf{k}\rangle$ which represents a two-nucleon state with definite total CM momentum $\mathbf{K}_{\rm CM}$ and relative one $\mathbf{k}$, we obtain

$$G|\mathbf{K}_{\rm CM}, \mathbf{k}\rangle = V|\mathbf{K}_{\rm CM}, \mathbf{k}\rangle + V\,\frac{Q}{E - H_0}\,G|\mathbf{K}_{\rm CM}, \mathbf{k}\rangle. \quad \text{(A1)}$$

If we use now the definition of the G matrix or effective interaction

$$G\underbrace{|\mathbf{K}_{\rm CM}, \mathbf{k}\rangle}_{\substack{\text{unperturbed}\\ \text{state}}} \equiv V\underbrace{|\Psi_{\mathbf{K}_{\rm CM},\mathbf{k}}\rangle}_{\substack{\text{perturbed}\\ \text{state}}}, \quad \text{(A2)}$$

which means that the action of the effective interaction over the unperturbed state is the same as the action of the potential over the corresponding perturbed state, then Eq. (A1) transforms into

$$V|\Psi_{\mathbf{K}_{\rm CM},\mathbf{k}}\rangle = V|\mathbf{K}_{\rm CM}, \mathbf{k}\rangle + V\,\frac{Q}{E - H_0}\,V|\Psi_{\mathbf{K}_{\rm CM},\mathbf{k}}\rangle, \quad \text{(A3)}$$

where E is the energy eigenvalue of the perturbed two-nucleon state $|\Psi_{\mathbf{K}_{\rm CM},\mathbf{k}}\rangle$, and $H_0 = T_1 + T_2$ is the unperturbed Hamiltonian containing only the one-body kinetic energy operators.

Formally, in Eq. (A3), assuming that V is invertible, we can act from the left by the inverse potential operator V^{-1}, thus eliminating the first appearance of the potential operator in all the terms of the equation. Additionally, we can also introduce a resolution of the identity operator in terms of the direct product of two single-particle momentum eigenstates, $\mathbf{I} = \int d^3k_1\, d^3k_2 |\mathbf{k}_1, \mathbf{k}_2\rangle\langle \mathbf{k}_1, \mathbf{k}_2|$, in between the $\frac{Q}{E-H_0}$ and V operators. With this, Eq. (A3) becomes

$$|\Psi_{\mathbf{K}_{\rm CM},\mathbf{k}}\rangle = |\mathbf{K}_{\rm CM}, \mathbf{k}\rangle + \int d^3k_1\, d^3k_2 \times \frac{\theta(|\mathbf{k}_1| - k_F)\,\theta(|\mathbf{k}_2| - k_F)}{E - (T_{\mathbf{k}_1} + T_{\mathbf{k}_2})} \times |\mathbf{k}_1, \mathbf{k}_2\rangle\langle \mathbf{k}_1, \mathbf{k}_2|V|\Psi_{\mathbf{K}_{\rm CM},\mathbf{k}}\rangle, \quad \text{(A4)}$$

where the two step functions come from the action of the Pauli-blocking operator Q over the two-particle momentum eigenstates $|\mathbf{k}_1, \mathbf{k}_2\rangle$, and $T_{\mathbf{k}_i} = \frac{\mathbf{k}_i^2}{2M_N}$ (with $i = 1, 2$) are the kinetic energy eigenvalues.

Again, in Eq. (A4), we can introduce another resolution of the identity operator in terms of the CM and relative momenta eigenstates representation, $\mathbf{I} = \int d^3K'_{\rm CM}\, d^3k' |\mathbf{K}'_{\rm CM}, \mathbf{k}'\rangle\langle \mathbf{K}'_{\rm CM}, \mathbf{k}'|$, in between the bra $\langle \mathbf{k}_1, \mathbf{k}_2|$ and the potential V operator. In this way, we obtain

$$|\Psi_{\mathbf{K}_{\rm CM},\mathbf{k}}\rangle = |\mathbf{K}_{\rm CM}, \mathbf{k}\rangle + \int d^3k_1\, d^3k_2 \times \frac{\theta(|\mathbf{k}_1| - k_F)\,\theta(|\mathbf{k}_2| - k_F)}{E - \left(T_{\mathbf{k}_1} + T_{\mathbf{k}_2}\right)} \times |\mathbf{k}_1, \mathbf{k}_2\rangle \int d^3K'_{\rm CM}\, d^3k' \langle \mathbf{k}_1, \mathbf{k}_2|\mathbf{K}'_{\rm CM}, \mathbf{k}'\rangle \times \langle \mathbf{K}'_{\rm CM}, \mathbf{k}'|V|\Psi_{\mathbf{K}_{\rm CM},\mathbf{k}}\rangle. \quad \text{(A5)}$$

Finally, using the first line for the bra-ket product $\langle \mathbf{k}_1, \mathbf{k}_2|\mathbf{K}'_{\rm CM}, \mathbf{k}'\rangle$ given in Eqs. (3), we can easily perform in Eq. (A5) the integrations over $\mathbf{k}_1$ and $\mathbf{k}_2$ with the aid of the two Dirac delta functions, obtaining

$$|\Psi_{\mathbf{K}_{\rm CM},\mathbf{k}}\rangle = |\mathbf{K}_{\rm CM}, \mathbf{k}\rangle + \int d^3K'_{\rm CM}\, d^3k' \frac{Q(\mathbf{K}'_{\rm CM}, \mathbf{k}')}{E - \left(\frac{\mathbf{K}'^2_{\rm CM}}{4M_N} + \frac{\mathbf{k}'^2}{M_N}\right)} \times \left|\frac{\mathbf{K}'_{\rm CM}}{2} + \mathbf{k}', \frac{\mathbf{K}'_{\rm CM}}{2} - \mathbf{k}'\right\rangle \times \langle \mathbf{K}'_{\rm CM}, \mathbf{k}'|V|\Psi_{\mathbf{K}_{\rm CM},\mathbf{k}}\rangle. \quad \text{(A6)}$$

In Eq. (A6), $Q(\mathbf{K}'_{\rm CM}, \mathbf{k}')$ stands for the two step functions written in terms of the CM and relative momenta [see Eq. (6)].

The final step to get Eq. (5) of Sec. II A is to assume that the true energy eigenvalue E of the perturbed state does not change too much from the energy eigenvalue of the unperturbed initial state, i.e., $E \simeq \frac{\mathbf{K}^2_{\rm CM}}{4M_N} + \frac{\mathbf{k}^2}{M_N}$, and to write the energy denominator in Eq. (A6) in terms of the total and reduced masses of the two-nucleon system. This approximation for the true energy eigenvalue has also been done by other authors, such as Ref. [134] in the context of the independent pair approximation.

The next step to obtain Eq. (7) of Sec. II A consists in trying to remove as much as possible the dependence on the CM momentum in Eq. (A6). For this to be possible it is completely necessary to assume that the potential does not depend at all on the CM coordinate; we will further assume that it is also local in the relative coordinate as well, as given in Eq. (4). To this end, we may introduce two resolutions of the identity

operator, one in terms of the CM and relative momenta eigenkets representation $\mathbf{I} = \int d^3K''_{\rm CM}\, d^3k''|\mathbf{K}''_{\rm CM}, \mathbf{k}''\rangle\langle\mathbf{K}''_{\rm CM}, \mathbf{k}''|$ inside the term with the integrals in Eq. (A6) and acting from the left on the $|\frac{\mathbf{K}'_{\rm CM}}{2} + \mathbf{k}', \frac{\mathbf{K}'_{\rm CM}}{2} - \mathbf{k}'\rangle$ ket, and the other one in terms of the CM and relative position eigenkets, $\mathbf{I} = \int d^3R'_{\rm CM}\, d^3r'|\mathbf{R}'_{\rm CM}, \mathbf{r}'\rangle\langle\mathbf{R}'_{\rm CM}, \mathbf{r}'|$, and acting in between the potential V operator and the perturbed state in Eq. (A6) as well:

$$|\Psi_{\mathbf{K}_{\rm CM},\mathbf{k}}\rangle = |\mathbf{K}_{\rm CM}, \mathbf{k}\rangle + \int d^3K'_{\rm CM}\, d^3k' \frac{Q(\mathbf{K}'_{\rm CM}, \mathbf{k}')}{\frac{(\mathbf{K}^2_{\rm CM}-\mathbf{K}'^2_{\rm CM})}{2M_T} + \frac{(\mathbf{k}^2-\mathbf{k}'^2)}{2\mu}} \int d^3K''_{\rm CM}\, d^3k''|\mathbf{K}''_{\rm CM}, \mathbf{k}''\rangle\, \delta^3\left(\frac{\mathbf{K}'_{\rm CM} - \mathbf{K}''_{\rm CM}}{2} + \mathbf{k}'' - \mathbf{k}'\right)$$
$$\times\, \delta^3\left(\frac{\mathbf{K}'_{\rm CM} - \mathbf{K}''_{\rm CM}}{2} + \mathbf{k}' - \mathbf{k}''\right) \int d^3R'_{\rm CM}\, d^3r'\;\; V(\mathbf{r}')\langle\mathbf{K}'_{\rm CM}, \mathbf{k}'|\mathbf{R}'_{\rm CM}, \mathbf{r}'\rangle\langle\mathbf{R}'_{\rm CM}, \mathbf{r}'|\Psi_{\mathbf{K}_{\rm CM},\mathbf{k}}\rangle. \tag{A7}$$

The two Dirac delta functions in Eq. (A7) come from the bra-ket product $\langle\mathbf{K}''_{\rm CM}, \mathbf{k}''|\frac{\mathbf{K}'_{\rm CM}}{2} + \mathbf{k}', \frac{\mathbf{K}'_{\rm CM}}{2} - \mathbf{k}'\rangle$, where the first line of the bra-ket product $\langle\mathbf{K}_{\rm CM}, \mathbf{k}|\mathbf{k}_1, \mathbf{k}_2\rangle$ given in Eqs. (3) was used with $\mathbf{k}_1 = \frac{\mathbf{K}'_{\rm CM}}{2} + \mathbf{k}'$ and $\mathbf{k}_2 = \frac{\mathbf{K}'_{\rm CM}}{2} - \mathbf{k}'$, and accordingly for the doubly primed CM and relative momenta variables of the bra.

To further proceed with Eq. (A7), it is necessary to pass from ket notation to wave function notation, in order to remove totally all the integrals over CM coordinates and momenta. To this end, we multiply both sides of Eq. (A7) from the left by the bra $\langle\mathbf{R}_{\rm CM}, \mathbf{r}|$; we also use the final line of Eqs. (3) for the unperturbed or plane wave states and

$$\langle\mathbf{R}_{\rm CM}, \mathbf{r}|\,\Psi_{\mathbf{K}_{\rm CM},\mathbf{k}}\rangle = \frac{e^{i\,\mathbf{K}_{\rm CM}\cdot\mathbf{R}_{\rm CM}}}{(2\pi)^{\frac{3}{2}}}\;\frac{\psi_{\mathbf{K}_{\rm CM},\mathbf{k}}(\mathbf{r})}{(2\pi)^{\frac{3}{2}}} \tag{A8}$$

for the perturbed wave functions in coordinate representation. It is worth noting that the plane wave for the CM motion in Eq. (A8) appears because the potential does not depend on the CM coordinate and it is, therefore, a constant of motion in our problem. Then, substituting the plane waves and Eq. (A8) into Eq. (A7), we can straightforwardly carry out the integrals over $\mathbf{k}''$, $\mathbf{R}'_{\rm CM}$, $\mathbf{K}'_{\rm CM}$ and $\mathbf{K}''_{\rm CM}$ in Eq. (A7). The final result is

$$\frac{e^{i\,\mathbf{K}_{\rm CM}\cdot\mathbf{R}_{\rm CM}}}{(2\pi)^{\frac{3}{2}}}\;\frac{\psi_{\mathbf{K}_{\rm CM},\mathbf{k}}(\mathbf{r})}{(2\pi)^{\frac{3}{2}}} = \frac{e^{i\,\mathbf{K}_{\rm CM}\cdot\mathbf{R}_{\rm CM}}}{(2\pi)^{\frac{3}{2}}}\;\frac{e^{i\,\mathbf{k}\cdot\mathbf{r}}}{(2\pi)^{\frac{3}{2}}} + \frac{e^{i\,\mathbf{K}_{\rm CM}\cdot\mathbf{R}_{\rm CM}}}{(2\pi)^{\frac{3}{2}}}\int d^3k'\;\frac{Q(\mathbf{K}_{\rm CM}, \mathbf{k}')}{k^2 - k'^2}\;\frac{e^{i\,\mathbf{k}'\cdot\mathbf{r}}}{(2\pi)^{\frac{3}{2}}}\int d^3r'\;\frac{e^{-i\,\mathbf{k}'\cdot\mathbf{r}'}}{(2\pi)^{\frac{3}{2}}}\;2\mu\,V(\mathbf{r}')\;\frac{\psi_{\mathbf{K}_{\rm CM},\mathbf{k}}(\mathbf{r}')}{(2\pi)^{\frac{3}{2}}}. \tag{A9}$$

In Eq. (A9) the plane wave for the CM motion cancels on both sides, and what remains is an integral B-G equation for the "single" particle relative wave function $\psi_{\mathbf{K}_{\rm CM},\mathbf{k}}(\mathbf{r})$, which can also be written as

$$\langle\mathbf{r}|\psi_{\mathbf{K}_{\rm CM},\mathbf{k}}\rangle = \langle\mathbf{r}|\mathbf{k}\rangle + \int d^3k'\;\frac{Q(\mathbf{K}_{\rm CM}, \mathbf{k}')}{k^2 - k'^2}\;\langle\mathbf{r}|\mathbf{k}'\rangle\int d^3r'\;\langle\mathbf{k}'|\mathbf{r}'\rangle\;2\mu\,V(\mathbf{r}')\;\langle\mathbf{r}'|\psi_{\mathbf{K}_{\rm CM},\mathbf{k}}\rangle$$
$$= \langle\mathbf{r}|\,\mathbf{k}\rangle + \langle\mathbf{r}|\int d^3k'\;\frac{Q(\mathbf{K}_{\rm CM}, \mathbf{k}')}{k^2 - k'^2}\;|\mathbf{k}'\rangle\,\langle\mathbf{k}'|\underbrace{\left(\int d^3r'\;2\mu\,V(\mathbf{r}')\;|\mathbf{r}'\rangle\,\langle\mathbf{r}'|\right)}_{\substack{\text{spectral resolution of the}\\ 2\mu\,V\text{ operator}}}|\psi_{\mathbf{K}_{\rm CM},\mathbf{k}}\rangle. \tag{A10}$$

Finally, in Eq. (A10), the bra $\langle\mathbf{r}|$ is arbitrary and appears on both sides of the equation. That bra can be removed from both sides and what remains is an integral equation for the ket $|\psi_{\mathbf{K}_{\rm CM},\mathbf{k}}\rangle$, which is precisely Eq. (7) of Sec. II A.

APPENDIX B: FORMAL DERIVATION OF THE INTEGRAL B-G EQUATION FOR THE RADIAL PART OF THE RELATIVE WAVE FUNCTION

Our aim in this Appendix is to obtain Eq. (10) of Sec. II C by performing a partial wave expansion of Eq. (7) in Sec. II A, but having substituted the general Pauli-blocking function $Q(\mathbf{K}_{\rm CM}, \mathbf{k}')$ by its angular average $\overline{Q}(K_{\rm CM}, k')$ given in Eq. (9).

Until now, all the discussion given in Appendix A has omitted the spin of the single-particle states or the total spin of the two-nucleon system. The latter can be totally ascribed to the relative kets $|\psi_{\mathbf{K}_{\rm CM},\mathbf{k}}\rangle$ and $|\mathbf{k}\rangle$ in Eq. (7). This last equation is an integral equation for the perturbed ket $|\psi_{\mathbf{K}_{\rm CM},\mathbf{k}}\rangle$, i.e., the same state appears on the left-hand side of the equation and on the right-hand one.

Additionally, it is a well-known fact that the N-N potential conserves the total spin S of the nucleon pair, its total angular momentum J, and the third component of the latter M, but neither the third component of the total spin M_S nor the orbital angular momenta, which can get mixed by the tensor force of the N-N potential. We start from Eq. (7) by substituting the Pauli-blocking function by its angular average, putting the spin and its third component on

the unperturbed and perturbed states, and now the resolution of the identity in terms of the momentum eigenkets is $\mathbf{I} = \sum_{S',M'_S} \int d^3k' |\mathbf{k}';S'M'_S\rangle\langle\mathbf{k}';S'M'_S|$:

$$|\psi_{\mathbf{k}};SM_S\rangle_{K_{\rm CM}} = |\mathbf{k};SM_S\rangle + \sum_{S',M'_S} \int d^3k' \, \frac{\overline{Q}(K_{\rm CM},k')}{k^2-k'^2} \times |\mathbf{k}';S'M'_S\rangle \, \langle\mathbf{k}';S'M'_S|2\mu\, V|\psi_{\mathbf{k}},SM_S\rangle_{K_{\rm CM}}. \tag{B1}$$

We know that for a large family of N-N potentials they have the properties of being local, preserving the total spin S, the total angular momentum J, and its third component M, but that due to the tensor force they mix orbital angular momenta. This means that we can write the spectral resolution of the potential as

$$V = \int_0^\infty dr\, r^2 \sum_{l,l'} \sum_{S,J,M} V^{SJ}_{ll'}(r) |r;lS;JM\rangle\langle r;l'S;JM|, \tag{B2}$$

where the basis $|r;lS;JM\rangle$ is given in terms of the eigenbasis of position and spin, $|\mathbf{r};SM_S\rangle$, as

$$|r;lS;JM\rangle = \sum_{m,M_S} \int d\Omega_{\hat{r}}\, Y_{lm}(\hat{r})\langle lm;SM_S|JM\rangle \, |\mathbf{r};SM_S\rangle. \tag{B3}$$

The spectral resolution of the potential given in Eq. (B2) ensures that its matrix elements between eigenkets of the form given in Eq. (B3) is

$$\langle r';l_1S_1;J_1M_1|V|r'';l_2S_2;J_2M_2\rangle = \delta_{S_1,S_2}\,\delta_{J_1,J_2}\,\delta_{M_1,M_2}\frac{1}{r'\,r''}\,\delta(r'-r'')\,V^{S_1J_1}_{l_1l_2}(r'), \tag{B4}$$

which is the obvious result for a local radial potential which preserves spin, total angular momentum, and its third component, but it is not necessarily diagonal in the orbital angular momentum. To derive Eq. (B4) we have used the orthogonality condition of the eigenbasis $|r;lS;JM\rangle$:

$$\langle r';l_1S_1;J_1M_1|r;lS;JM\rangle = \frac{1}{r\,r'}\,\delta(r-r')\,\delta_{l,l_1}\delta_{S,S_1}\delta_{J,J_1}\delta_{M,M_1}, \tag{B5}$$

which in turn can be obtained by evaluating the bra-ket product with the expansion of the eigenbasis given in Eq. (B3) and using the more obvious orthogonality condition of the eigenbasis of position and spin $|\mathbf{r};SM_S\rangle$.

Introducing the spectral resolution of the potential, Eq. (B2), into the bra-ket product of Eq. (B1), we obtain

$$\langle\mathbf{k}';S'M'_S|2\mu\, V|\psi_{\mathbf{k}},SM_S\rangle_{K_{\rm CM}} = \int_0^\infty dr\, r^2 \sum_{l,l'}\sum_{S''JM} 2\mu V^{S''J}_{ll'}(r) \times \frac{4\pi}{(2\pi)^{\frac{3}{2}}}\,\delta_{S'',S'}\, i^{-l}\, j_l(k'r) \sum_m Y_{lm}(\hat{k}')\langle lm;S''M'_S|JM\rangle \times \left(\int d^3r' \langle r;l'S'';JM|\mathbf{r}'\rangle\langle\mathbf{r}'|\psi_{\mathbf{k}},SM_S\rangle_{K_{\rm CM}} \right), \tag{B6}$$

where in the last piece between parenthesis we have introduced a resolution of the identity in the form $\int d^3r'|\mathbf{r}'\rangle\langle\mathbf{r}'|$, and we have also used that

$$\langle\mathbf{k}';S'M'_S|r;lS'';JM\rangle = \frac{4\pi}{(2\pi)^{\frac{3}{2}}}\,\delta_{S'',S'}\, i^{-l}\, j_l(k'r) \times \sum_m Y_{lm}(\hat{k}')\langle lm;S''M'_S|JM\rangle. \tag{B7}$$

This last expression can be easily obtained by multiplying Eq. (B3) from the left by the bra $\langle\mathbf{k}';S'M'_S|$, using the Rayleigh expansion for the plane wave, and carrying out the calculations.

In Eq. (B6) we can substitute Eq. (21) for the correlated wave function in coordinate representation, and the bra-ket product

$$\langle r;l'S'';JM|\mathbf{r}'\rangle = \frac{1}{r\,r'}\,\delta(r-r')\,\mathcal{Y}^\dagger_{l'S''JM}(\hat{r}'), \tag{B8}$$

where this last equation can be easily obtained from Eq. (B3) by multiplying from the left by a position eigenstate, carrying out the calculations, and taking its complex conjugate.

Carrying out the calculations of the piece between parenthesis of Eq. (B6) we obtain finally

$$\int d^3r' \langle r;l'S'';JM|\mathbf{r}'\rangle\langle\mathbf{r}'|\psi_{\mathbf{k}},SM_S\rangle_{K_{\rm CM}} = \frac{4\pi}{(2\pi)^{\frac{3}{2}}} \sum_{l''m''} i^{l''}\, u^{SJ}_{k,l''l'}(r)\, Y^*_{l''m''}(\hat{k})\,\delta_{S,S''}\langle l''m'';SM_S|JM\rangle, \tag{B9}$$

where to obtain the above result we have integrated over r' with the aid of the Dirac delta function of Eq. (B8), and we have also used the orthogonality properties of the spin-angular wave functions, namely

$$\int d\Omega_{\hat{r}'}\, \mathcal{Y}^*_{l'S''JM}(\hat{r}')\,\mathcal{Y}_{lSJ'M'}(\hat{r}') = \delta_{l',l}\,\delta_{S'',S}\,\delta_{J,J'}\,\delta_{M,M'}, \tag{B10}$$

in order to carry out some discrete sums over J', M', l in the expansion of the perturbed wave function in partial waves, given by Eq. (21).

Introducing the result of Eq. (B9) into Eq. (B6), we obtain finally

$$\langle\mathbf{k}';S'M'_S|2\mu\, V|\psi_{\mathbf{k}},SM_S\rangle_{K_{\rm CM}} = \frac{(4\pi)^2}{(2\pi)^3}\,\delta_{S,S'}\sum_{l,l'm}\sum_{JM}\sum_{l''m''} i^{l''-l} \times Y_{lm}(\hat{k}')\, Y^*_{l''m''}(\hat{k})\langle lm;SM'_S|JM\rangle\langle l''m'';SM_S|JM\rangle \times \int_0^\infty dr'\, r'^2\, U^{SJ}_{ll'}(r')\, j_l(k'r')\, u^{SJ}_{k,l''l'}(r'), \tag{B11}$$

where $U^{SJ}_{ll'} = 2\mu V^{SJ}_{ll'}$ is the reduced potential.

If we now introduce the matrix element so far calculated in Eq. (B11) in the B-G equation for the relative ket, Eq. (B1), multiply from the left by the position eigenbra $\langle\mathbf{r}|$, and substitute Eqs. (19) and (21) for the expansions of the free and perturbed wave functions in coordinates representation, we

have Eq. (21) on the left-hand side (LHS), while on the right-hand side we have

$$\begin{aligned}\text{LHS} = &\frac{4\pi}{(2\pi)^{\frac{3}{2}}}\sum_{JM}\sum_{l\,l'm} i^{l'}\, j_{l'}(kr)\,\delta_{l'l}\,Y^*_{l'm}(\hat{k})\langle l'm;SM_S|JM\rangle\mathcal{Y}_{lSJM}(\hat{r}) + \sum_{S',M'_S}\int d^3k'\,\frac{\overline{Q}(K_{\text{CM}},k')}{k^2-k'^2}\left(\frac{4\pi}{(2\pi)^{\frac{3}{2}}}\sum_{J'M'}\sum_{l_1l'_1m_1} i^{l'_1}\right.\\ &\left.\times\, j_{l'_1}(k'r)\,\delta_{l'_1l_1}Y^*_{l'_1m_1}(\hat{k}')\langle l'_1m_1;S'M'_S|J'M'\rangle\mathcal{Y}_{l_1S'J'M'}(\hat{r})\right)\left(\frac{(4\pi)^2}{(2\pi)^3}\,\delta_{S,S'}\sum_{l,l'm}\sum_{JM}\sum_{l''m''} i^{l''-l}\,Y_{lm}(\hat{k}')\,Y^*_{l''m''}(\hat{k})\right.\\ &\left.\times\,\langle lm;SM'_S|JM\rangle\langle l''m'';SM_S|JM\rangle\int_0^\infty dr'\,r'^2\,U^{SJ}_{ll'}(r')j_l(k'r')\,u^{SJ}_{k,l''l'}(r')\right).\end{aligned} \tag{B12}$$

In the second term of the above equation we can carry out the sum over S' because of the presence of the Kronecker delta $\delta_{S,S'}$. In addition, we can carry out the integration over the angles of $\hat{k}'$ exploiting the orthogonality of the spherical harmonics of $\hat{k}'$, thus obtaining $\delta_{l'_1l}\,\delta_{m_1m}$, and carry out the additional sums over l'_1 and m_1, obtaining at the end

$$\begin{aligned}\text{LHS} = &\frac{4\pi}{(2\pi)^{\frac{3}{2}}}\sum_{JM}\sum_{l\,l'm} i^{l'}\, j_{l'}(kr)\,\delta_{l'l}\,Y^*_{l'm}(\hat{k})\langle l'm;SM_S|JM\rangle\mathcal{Y}_{lSJM}(\hat{r}) + \frac{(4\pi)^3}{(2\pi)^{\frac{9}{2}}}\sum_{M'_S=-S}^{S}\sum_{J'M'}\sum_{JM}\sum_{l,l'm}\sum_{l''m''}\sum_{l_1} i^{l''}\,\delta_{l,l_1}\\ &\times\langle lm;SM'_S|J'M'\rangle\langle lm;SM'_S|JM\rangle\langle l''m'';SM_S|JM\rangle Y^*_{l''m''}(\hat{k})\;\mathcal{Y}_{l_1SJ'M'}(\hat{r})\int_0^\infty dk'\,k'^2\,\frac{\overline{Q}(K_{\text{CM}},k')}{k^2-k'^2}\,j_l(k'r)\\ &\times\int_0^\infty dr'\,r'^2\,U^{SJ}_{ll'}(r')\;j_l(k'r')\,u^{SJ}_{k,l''l'}(r').\end{aligned} \tag{B13}$$

Again, in the second term of Eq. (B13) we can perform easily the sum over l_1. Furthermore, the sum over m and M'_S for fixed (l,S,J,M,J',M') only involves two Clebsch-Gordan coefficients and its result is $\delta_{JJ'}\,\delta_{MM'}$, and we can then carry out the sum over J' and M', obtaining

$$\begin{aligned}\text{LHS} = &\frac{4\pi}{(2\pi)^{\frac{3}{2}}}\sum_{JM}\sum_{l\,l'm} i^{l'}\, j_{l'}(kr)\,\delta_{l'l}\,Y^*_{l'm}(\hat{k})\langle l'm;SM_S|JM\rangle\mathcal{Y}_{lSJM}(\hat{r}) + \frac{(4\pi)^3}{(2\pi)^{\frac{9}{2}}}\sum_{JM}\sum_{l,l'}\sum_{l''m''} i^{l''}\langle l''m'';SM_S|JM\rangle\;Y^*_{l''m''}(\hat{k})\\ &\times\mathcal{Y}_{lSJM}(\hat{r})\int_0^\infty dr'\,\frac{kr'}{kr}\,U^{SJ}_{ll'}(r')\,u^{SJ}_{k,l''l'}(r')\int_0^\infty dk'\,(k'r')\,j_l(k'r')\,\frac{\overline{Q}(K_{\text{CM}},k')}{k^2-k'^2}\,(k'r')\,j_l(k'r').\end{aligned} \tag{B14}$$

Finally, the second term of Eq. (B14) can be arranged in the final form

$$\begin{aligned}\text{LHS} = &\frac{4\pi}{(2\pi)^{\frac{3}{2}}}\sum_{JM}\sum_{l\,l'm} i^{l'}\, j_{l'}(kr)\,\delta_{l'l}\,Y^*_{l'm}(\hat{k})\langle l'm;SM_S|JM\rangle\mathcal{Y}_{lSJM}(\hat{r}) + \frac{(4\pi)}{(2\pi)^{\frac{3}{2}}}\sum_{JM}\sum_{l,l''}\sum_{l'm} i^{l'}\langle l'm;SM_S|JM\rangle\;Y^*_{l'm}(\hat{k})\\ &\times\mathcal{Y}_{lSJM}(\hat{r})\int_0^\infty dr'\,U^{SJ}_{ll''}(r')\,\frac{\widetilde{u}^{SJ}_{k,l'l''}(r')}{kr}\,\underbrace{\frac{2}{\pi}\int_0^\infty dk'\;\hat{j}_l(k'r')\,\frac{\overline{Q}(K_{\text{CM}},k')}{k^2-k'^2}\,\hat{j}_l(k'r')}_{\widetilde{G}^{K_{\text{CM}}}_{k,l}(r,r')},\end{aligned} \tag{B15}$$

where in Eq. (B15) we have used the definition of the Green's function for the radial B-G equation, given in Eq. (11), and the normalization of the perturbed radial wave function given in Eq. (22) has also been used. Finally, also in the second term of Eq. (B15) the labels $l'\leftrightarrow l''$ and $m''\to m$ have been renamed in the sums.

Therefore, at the end, we have on both sides of the equation

$$\begin{aligned}&\frac{4\pi}{(2\pi)^{\frac{3}{2}}}\sum_{J,M}\sum_{l,l',m} i^{l'}\,u^{SJ}_{k,l'l}(r)\,Y^*_{l'm}(\hat{k})\langle l'm;SM_S|JM\rangle\;\mathcal{Y}_{lSJM}(\hat{r})\\ &=\frac{4\pi}{(2\pi)^{\frac{3}{2}}}\sum_{JM}\sum_{l\,l'm} i^{l'}\, j_{l'}(kr)\,\delta_{l'l}\,Y^*_{l'm}(\hat{k})\langle l'm;SM_S|JM\rangle\mathcal{Y}_{lSJM}(\hat{r}) + \frac{4\pi}{(2\pi)^{\frac{3}{2}}}\sum_{JM}\sum_{ll'm}\sum_{l''} i^{l'}\langle l'm;SM_S|JM\rangle Y^*_{l'm}(\hat{k})\;\mathcal{Y}_{lSJM}(\hat{r})\\ &\times\int_0^\infty dr'\,\widetilde{G}^{K_{\text{CM}}}_{k,l}(r,r')\,U^{SJ}_{ll''}(r')\,\frac{\widetilde{u}^{SJ}_{k,l'l''}(r')}{kr}.\end{aligned} \tag{B16}$$

Obviously, the factors cancel on both sides, and to obtain the equation for the radial part we have to get rid of all the angular dependencies on $\hat{k}$ and $\hat{r}$. To this end, we can multiply from the left by the spin-angular wave function $\mathcal{Y}^\dagger_{l_1S_1J_1M_1}(\hat{r})$ and integrate

over the solid angle of $\hat{r}$. Using the orthogonality properties of these functions we can perform trivially the sums over l, J, and M:

$$\delta_{S,S_1}\sum_{l'm} i^{l'}\, u^{SJ_1}_{k,l'\,l_1}(r)\, Y^*_{l'm}(\hat{k})\langle l'm; SM_S|J_1M_1\rangle = \delta_{S,S_1}\sum_{l'm} i^{l'}\, j_{l'}(kr)\,\delta_{l'l_1}\, Y^*_{l'm}(\hat{k})\langle l'm; SM_S|J_1M_1\rangle$$
$$+\,\delta_{S,S_1}\sum_{l'm}\sum_{l''} i^{l'}\,\langle l'm; SM_S|J_1M_1\rangle Y^*_{l'm}(\hat{k})\int_0^\infty dr'\,\widetilde{G}^{K_{\rm CM}}_{k,l_1}(r,r')\,U^{SJ_1}_{l_1l''}(r')\,\frac{\widetilde{u}^{SJ_1}_{k,l'\,l''}(r')}{kr}. \tag{B17}$$

We can take without loss of generality that $S_1 = S$ to get rid of the Kronecker deltas. Then, we can multiply on both sides of Eq. (B17) by $Y_{lm'}(\hat{k})$ and integrate over the solid angle of $\hat{k}$. Using the orthogonality of the spherical harmonics, we can carry out the sum over l' and m, thus obtaining finally

$$u^{SJ}_{k,l\,l'}(r) = j_l(kr)\,\delta_{l,l'} + \int_0^\infty dr'\,\widetilde{G}^{K_{\rm CM}}_{k,l'}(r,r')\sum_{l''} U^{SJ}_{l'l''}(r')\,\frac{\widetilde{u}^{SJ}_{k,l\,l''}(r')}{kr}, \tag{B18}$$

where in Eq. (B18) we have canceled the Clebsch-Gordan coefficients after having carried out the sum over l' and m because they were the same on both sides of the equation. And finally we have renamed the free indices $J_1 \to J$, and $l_1 \to l'$ on both sides of the equation after having performed the sums. Finally, if we multiply both sides by kr, we obtain the B-G equation for the perturbed (correlated) relative radial wave function [see Eq. (10)]:

$$\widetilde{u}^{SJ}_{k,l\,l'}(r) = \hat{j}_l(kr)\,\delta_{l,l'} + \int_0^\infty dr'\,\widetilde{G}^{K_{\rm CM}}_{k,l'}(r,r')\sum_{l''} U^{SJ}_{l'l''}(r')\,\widetilde{u}^{SJ}_{k,l\,l''}(r'). \tag{B19}$$

[1] D. Hartree, Math. Proc. Cambridge Philos. Soc. **24**, 89 (1928).
[2] D. Hartree, Math. Proc. Cambridge Philos. Soc. **24**, 111 (1928).
[3] R. Jastrow, Phys. Rev. **79**, 389 (1950).
[4] R. Jastrow, Phys. Rev. **81**, 165 (1951).
[5] R. Jastrow, Phys. Rev. **98**, 1479 (1955).
[6] K. A. Brueckner, R. J. Eden, and N. C. Francis, Phys. Rev. **98**, 1445 (1955).
[7] H. A. Bethe, Phys. Rev. **103**, 1353 (1956).
[8] H. A. Bethe and J. Goldstone, Proc. R. Soc. London. A **238**, 551 (1957).
[9] K. A. Brueckner and J. L. Gammel, Phys. Rev. **109**, 1023 (1958).
[10] H. A. Bethe, Phys. Rev. **138**, B804 (1965).
[11] C. W. Leemann, D. R. Douglas, and G. A. Krafft, Annu. Rev. Nucl. Part. Sci. **51**, 413 (2001).
[12] B. A. Mecking *et al.* (CLAS Collaboration), Nucl. Instrum. Methods Phys. Res. Sect. A **503**, 513 (2003).
[13] L. J. H. M. Kester *et al.*, Phys. Rev. Lett. **74**, 1712 (1995).
[14] J. J. van Leeuwe *et al.*, Phys. Rev. Lett. **80**, 2543 (1998).
[15] C. J. G. Onderwater *et al.*, Phys. Rev. Lett. **81**, 2213 (1998).
[16] K. I. Blomqvist *et al.*, Phys. Lett. B **421**, 71 (1998).
[17] R. Starink *et al.*, Phys. Lett. B **474**, 33 (2000).
[18] A. Tang *et al.*, Phys. Rev. Lett. **90**, 042301 (2003).
[19] K. S. Egiyan *et al.* (CLAS Collaboration), Phys. Rev. Lett. **96**, 082501 (2006).
[20] R. Shneor *et al.* (Jefferson Lab Hall A Collaboration), Phys. Rev. Lett. **99**, 072501 (2007).
[21] R. Subedi *et al.*, Science **320**, 1476 (2008).
[22] H. Baghdasaryan *et al.* (CLAS Collaboration), Phys. Rev. Lett. **105**, 222501 (2010).
[23] N. Fomin *et al.*, Phys. Rev. Lett. **108**, 092502 (2012).
[24] W. U. Boeglin *et al.* (Hall A Collaboration), Phys. Rev. Lett. **107**, 262501 (2011).
[25] O. Hen *et al.* (CLAS Collaboration), Phys. Lett. B **722**, 63 (2013).
[26] I. Korover *et al.* (Lab Hall A Collaboration), Phys. Rev. Lett. **113**, 022501 (2014).
[27] O. Hen *et al.*, Science **346**, 614 (2014).
[28] Z. Ye *et al.* (Hall A Collaboration), Phys. Rev. C **97**, 065204 (2018).
[29] E. O. Cohen *et al.* (CLAS Collaboration), Phys. Rev. Lett. **121**, 092501 (2018).
[30] R. Schiavilla, V. R. Pandharipande, and R. B. Wiringa, Nucl. Phys. A **449**, 219 (1986).
[31] A. Ramos, A. Polls, and W. H. Dickhoff, Nucl. Phys. A **503**, 1 (1989).
[32] B. E. Vonderfecht, W. H. Dickhoff, A. Polls, and A. Ramos, Nucl. Phys. A **555**, 1 (1993).
[33] L. L. Frankfurt, M. I. Strikman, D. B. Day, and M. Sargsyan, Phys. Rev. C **48**, 2451 (1993).
[34] M. V. Stoitsov, A. N. Antonov, and S. S. Dimitrova, Phys. Rev. C **48**, 74 (1993).
[35] H. Müther, A. Polls, and W. H. Dickhoff, Phys. Rev. C **51**, 3040 (1995).
[36] H. Müther, G. Knehr, and A. Polls, Phys. Rev. C **52**, 2955 (1995).
[37] J. Ryckebusch, M. Vanderhaeghen, K. Heyde, and M. Waroquier, Phys. Lett. B **350**, 1 (1995).
[38] C. Giusti, H. Muther, F. D. Pacati, and M. Stauf, Phys. Rev. C **60**, 054608 (1999).
[39] Y. Dewulf, W. H. Dickhoff, D. Van Neck, E. R. Stoddard, and M. Waroquier, Phys. Rev. Lett. **90**, 152501 (2003).
[40] R. Schiavilla, R. B. Wiringa, S. C. Pieper, and J. Carlson, Phys. Rev. Lett. **98**, 132501 (2007).
[41] M. Kortelainen, O. Civitarese, J. Suhonen, and J. Toivanen, Phys. Lett. B **647**, 128 (2007).

[42] M. Alvioli, C. Ciofi degli Atti, and H. Morita, Phys. Rev. Lett. **100**, 162503 (2008).
[43] R. B. Wiringa, R. Schiavilla, S. C. Pieper, and J. Carlson, Phys. Rev. C **78**, 021001(R) (2008).
[44] L. Frankfurt, M. Sargsian, and M. Strikman, Int. J. Mod. Phys. A **23**, 2991 (2008).
[45] L. B. Weinstein, E. Piasetzky, D. W. Higinbotham, J. Gomez, O. Hen, and R. Shneor, Phys. Rev. Lett. **106**, 052301 (2011).
[46] H. Feldmeier, W. Horiuchi, T. Neff, and Y. Suzuki, Phys. Rev. C **84**, 054003 (2011).
[47] M. M. Sargsian, Phys. Rev. C **89**, 034305 (2014).
[48] M. Alvioli, C. Ciofi degli Atti, L. P. Kaptari, C. B. Mezzetti, and H. Morita, Phys. Rev. C **87**, 034603 (2013).
[49] M. Vanhalst, J. Ryckebusch, and W. Cosyn, Phys. Rev. C **86**, 044619 (2012).
[50] R. B. Wiringa, R. Schiavilla, S. C. Pieper, and J. Carlson, Phys. Rev. C **89**, 024305 (2014).
[51] L. White and F. Sammarruca, Phys. Rev. C **88**, 054619 (2013).
[52] F. Sammarruca, Phys. Rev. C **90**, 064312 (2014).
[53] B.-J. Cai and B.-A. Li, Phys. Rev. C **93**, 014619 (2016).
[54] F. Sammarruca, Phys. Rev. C **92**, 044003 (2015).
[55] T. Neff, H. Feldmeier, and W. Horiuchi, Phys. Rev. C **92**, 024003 (2015).
[56] C. Colle, O. Hen, W. Cosyn, I. Korover, E. Piasetzky, J. Ryckebusch, and L. B. Weinstein, Phys. Rev. C **92**, 024604 (2015).
[57] M. Alvioli, C. Ciofi degli Atti, and H. Morita, Phys. Rev. C **94**, 044309 (2016).
[58] R. Weiss, R. Cruz-Torres, N. Barnea, E. Piasetzky, and O. Hen, Phys. Lett. B **780**, 211 (2018).
[59] J.-W. Chen, W. Detmold, J. E. Lynn, and A. Schwenk, Phys. Rev. Lett. **119**, 262502 (2017).
[60] U. Mosel and K. Gallmeister, Phys. Rev. C **94**, 034610 (2016).
[61] O. Artiles and M. M. Sargsian, Phys. Rev. C **94**, 064318 (2016).
[62] D. Ding, A. Rios, H. Dussan, W. H. Dickhoff, S. J. Witte, A. Carbone, and A. Polls, Phys. Rev. C **94**, 025802 (2016); **94**, 029901(E) (2016).
[63] I. Ruiz Simo, R. Navarro Perez, J. E. Amaro, and E. Ruiz Arriola, Phys. Rev. C **95**, 054003 (2017).
[64] R. Cruz-Torres, A. Schmidt, G. A. Miller, L. B. Weinstein, N. Barnea, R. Weiss, E. Piasetzky, and O. Hen, Phys. Lett. B **785**, 304 (2018).
[65] S. Stevens, J. Ryckebusch, W. Cosyn, and A. Waets, Phys. Lett. B **777**, 374 (2018).
[66] A. Rios, A. Polls, and W. H. Dickhoff, J. Low. Temp. Phys. **189**, 234 (2017).
[67] C. Ciofi degli Atti, C. B. Mezzetti, and H. Morita, Phys. Rev. C **95**, 044327 (2017).
[68] I. Ruiz Simo, R. Navarro Pérez, J. E. Amaro, and E. Ruiz Arriola, Phys. Rev. C **96**, 054006 (2017).
[69] J. Arrington, D. W. Higinbotham, G. Rosner, and M. Sargsian, Prog. Part. Nucl. Phys. **67**, 898 (2012).
[70] C. Ciofi degli Atti, Phys. Rep. **590**, 1 (2015).
[71] O. Hen, G. A. Miller, E. Piasetzky, and L. B. Weinstein, Rev. Mod. Phys. **89**, 045002 (2017).
[72] N. Fomin, D. Higinbotham, M. Sargsian, and P. Solvignon, Annu. Rev. Nucl. Part. Sci. **67**, 129 (2017).
[73] H. A. Bethe, Annu. Rev. Nucl. Sci. **21**, 93 (1971).
[74] J. P. Jeukenne, A. Lejeune, and C. Mahaux, Phys. Rep. **25**, 83 (1976).
[75] B. E. Vonderfecht, W. H. Dickhoff, A. Polls, and A. Ramos, Phys. Rev. C **44**, R1265 (1991).
[76] S. Fantoni and V. R. Pandharipande, Nucl. Phys. A **427**, 473 (1984).
[77] O. Benhar, C. Ciofi Degli Atti, S. Liuti, and G. Salmè, Phys. Lett. B **177**, 135 (1986).
[78] J. W. Van Orden, W. Truex, and M. K. Banerjee, Phys. Rev. C **21**, 2628 (1980).
[79] H. Riffert, H. Muther, H. Herold, and H. Ruder, *Matter at High Densities in Astrophysics*, Springer Tracts in Modern Physics Vol. 133 (Springer, Berlin, 1996).
[80] A. Mukherjee, Phys. Rev. C **79**, 045811 (2009).
[81] G. Shen, C. J. Horowitz, and S. Teige, Phys. Rev. C **83**, 035802 (2011).
[82] G. Röpke, Phys. Rev. C **92**, 054001 (2015).
[83] O. Hen, A. W. Steiner, E. Piasetzky, and L. B. Weinstein, arXiv:1608.00487.
[84] O. Hen, B.-A. Li, W.-J. Guo, L. B. Weinstein, and E. Piasetzky, Phys. Rev. C **91**, 025803 (2015).
[85] W. Broniowski and M. Rybczynski, Phys. Rev. C **81**, 064909 (2010).
[86] F. Šimkovic, A. Faessler, H. Muther, V. Rodin, and M. Stauf, Phys. Rev. C **79**, 055501 (2009).
[87] M. Kortelainen and J. Suhonen, Phys. Rev. C **76**, 024315 (2007).
[88] S. Tan, Ann. Phys. (NY) **323**, 2952 (2008).
[89] S. Tan, Ann. Phys. (NY) **323**, 2971 (2008).
[90] S. Tan, Ann. Phys. (NY) **323**, 2987 (2008).
[91] M. Alvioli, C. Ciofi degli Atti, L. P. Kaptari, C. B. Mezzetti, H. Morita, and S. Scopetta, Phys. Rev. C **85**, 021001(R) (2012).
[92] M. Alvioli, C. Ciofi degli Atti, L. P. Kaptari, C. B. Mezzetti, and H. Morita, Int. J. Mod. Phys. E **22**, 1330021 (2013).
[93] R. Weiss, B. Bazak, and N. Barnea, Phys. Rev. C **92**, 054311 (2015).
[94] R. Weiss and N. Barnea, Phys. Rev. C **96**, 041303(R) (2017).
[95] S. Fantoni and S. Rosati, Nuovo Cimento A **20**, 179 (1974).
[96] S. Fantoni and S. Rosati, Nuovo Cimento A **25**, 593 (1975).
[97] R. Guardiola, A. Polls, and J. Ros, Nuovo Cimento A **59**, 419 (1980).
[98] R. Guardiola, A. Faessler, H. Müther, and A. Polls, Nucl. Phys. A **371**, 79 (1981).
[99] O. Benhar, A. Fabrocini, and S. Fantoni, in *Modern Topics in Electron Scattering*, edited by B. Frois and I. Sick (World Scientific, Singapore, 1991), p. 460.
[100] O. Benhar, A. Fabrocini, S. Fantoni, and I. Sick, Nucl. Phys. A **579**, 493 (1994).
[101] R. Guardiola, P. I. Moliner, J. Navarro, R. F. Bishop, A. Puente, and N. R. Walet, Nucl. Phys. A **609**, 218 (1996).
[102] R. F. Bishop, R. Guardiola, I. Moliner, J. Navarro, M. Portesi, A. Puente, and N. R. Walet, Nucl. Phys. A **643**, 243 (1998).
[103] K. A. Brueckner, C. A. Levinson, and H. M. Mahmoud, Phys. Rev. **95**, 217 (1954).
[104] K. A. Brueckner, Phys. Rev. **97**, 1353 (1955).
[105] J. Goldstone, Proc. R. Soc. London A **239**, 267 (1957).
[106] G. Dahll, E. Østgaard, and B. Brandow, Nucl. Phys. A **124**, 481 (1969).
[107] H. S. Köhler, Ann. Phys. (NY) **16**, 375 (1961).
[108] M. I. Haftel and F. Tabakin, Nucl. Phys. A **158**, 1 (1970).

[109] J. P. Jeukenne, A. Lejeune, and C. Mahaux, Phys. Rev. C **10**, 1391 (1974).
[110] K. Nakayama, S. Krewald, J. Speth, and W. G. Love, Nucl. Phys. A **431**, 419 (1984).
[111] A. Hosaka, K. I. Kubo, and H. Toki, Nucl. Phys. A **444**, 76 (1985).
[112] K. Nakayama, S. Drozdz, S. Krewald, and J. Speth, Nucl. Phys. A **470**, 573 (1987); **484**, 685(E) (1988).
[113] H. F. Boersma and R. Malfliet, Phys. Rev. C **49**, 233 (1994); **50**, 1253(E) (1994).
[114] S. K. Bogner, R. J. Furnstahl, and R. J. Perry, Phys. Rev. C **75**, 061001(R) (2007).
[115] V. S. Timoteo, S. Szpigel, and E. Ruiz Arriola, Phys. Rev. C **86**, 034002 (2012).
[116] J. Carlson, V. R. Pandharipande, and R. Schiavilla, Phys. Rev. C **47**, 484 (1993).
[117] J. L. Forest, V. R. Pandharipande, J. Carlson, and R. Schiavilla, Phys. Rev. C **52**, 576 (1995).
[118] S. Quaglioni and P. Navratil, Phys. Rev. C **79**, 044606 (2009).
[119] G. Hagen, T. Papenbrock, D. J. Dean, and M. Hjorth-Jensen, Phys. Rev. C **82**, 034330 (2010).
[120] W. Leidemann and G. Orlandini, Prog. Part. Nucl. Phys. **68**, 158 (2013).
[121] B. R. Barrett, P. Navratil, and J. P. Vary, Prog. Part. Nucl. Phys. **69**, 131 (2013).
[122] R. D. Viollier and J. D. Walecka, Acta Phys. Pol. **B8**, 25 (1977).
[123] R. Navarro Pérez, J. E. Amaro, and E. Ruiz Arriola, Phys. Rev. C **88**, 024002 (2013); **88**, 069902(E) (2013).
[124] P. C. Bhargava and D. W. Sprung, Ann. Phys. (NY) **42**, 222 (1967).
[125] A. Kallio and B. D. Day, Nucl. Phys. A **124**, 177 (1969).
[126] D. Alonso and F. Sammarruca, Phys. Rev. C **67**, 054301 (2003).
[127] E. Werner, Nucl. Phys. **10**, 688 (1959).
[128] T. Cheon and E. F. Redish, Phys. Rev. C **39**, 331 (1989).
[129] E. Schiller, H. Muther, and P. Czerski, Phys. Rev. C **59**, 2934 (1999); **60**, 059901(E) (1999).
[130] K. Suzuki, R. Okamoto, M. Kohno, and S. Nagata, Nucl. Phys. A **665**, 92 (2000).
[131] F. Sammarruca, X. Meng, and E. J. Stephenson, Phys. Rev. C **62**, 014614 (2000).
[132] E. J. Stephenson, R. C. Johnson, and F. Sammarruca, Phys. Rev. C **71**, 014612 (2005).
[133] L. White and F. Sammarruca, Phys. Rev. C **90**, 044607 (2014).
[134] J. Walecka, *Theoretical Nuclear and Subnuclear Physics* (Oxford University Press, New York, 1995).
[135] R. N. Pérez, J. E. Amaro, and E. R. Arriola, Phys. Rev. C **88**, 064002 (2013); **91**, 029901(E) (2015).
[136] D. Levin, J. Comput. Appl. Math. **67**, 95 (1996).
[137] D. Levin, J. Comput. Appl. Math. **78**, 131 (1997).
[138] H. Moeini and G. H. Bordbar, Nucl. Phys. A **1017**, 122339 (2022).
[139] M. Kohno, Phys. Rev. C **88**, 064005 (2013); **96**, 059903(E) (2017).
[140] M. Kohno, Phys. Rev. C **86**, 061301(R) (2012).
[141] A. Lovato, O. Benhar, S. Fantoni, A. Y. Illarionov, and K. E. Schmidt, Phys. Rev. C **83**, 054003 (2011).
[142] J. W. Holt, N. Kaiser, and W. Weise, Phys. Rev. C **81**, 024002 (2010).
[143] N. Barnea, V. D. Efros, W. Leidemann, and G. Orlandini, Few Body Syst. **35**, 155 (2004).
[144] J. E. Amaro, R. Navarro Pérez, and E. Ruiz Arriola, 2013 Granada Database, http://www.ugr.es/~amaro/nndatabase/.
[145] R. B. Wiringa (private communication).
[146] M. Piarulli, S. Pastore, R. B. Wiringa, S. Brusilow, and R. Lim, Phys. Rev. C **107**, 014314 (2023).
[147] R. B. Wiringa, Two-Nucleon Momentum Distributions, 2023, https://www.phy.anl.gov/theory/research/momenta2/.
[148] J. Ryckebusch, W. Cosyn, and M. Vanhalst, J. Phys. G: Nucl. Part. Phys. **42**, 055104 (2015).